

## DISTANT COOLING FLOWS

MEGAN DONAHUE<sup>1,2</sup>, AND JOHN T. STOCKE<sup>1</sup>

Center for Astrophysics and Space Astronomy and Department of Astrophysical, Planetary, and Atmospheric Sciences,  
 University of Colorado, Boulder, CO 80309

AND

ISABELLA M. GIOIA<sup>3</sup>

Harvard-Smithsonian Center for Astrophysics, Cambridge, MA; and Istituto di Radioastronomia del CNR, Bologna, Italy

Received 1991 April 9; accepted 1991 July 29

### ABSTRACT

Luminous, extended H $\alpha$  emission has been detected in 14 distant X-ray–selected clusters of galaxies ( $0.07 < z < 0.37$ ). Eleven of these detections are from a complete flux-limited sample ( $f_x \geq 8 \times 10^{-13}$  ergs cm<sup>-2</sup> s<sup>-1</sup>,  $\delta \geq -20^\circ$ ) of 23 clusters extracted from the *Einstein* Extended Medium-Sensitivity Survey (EMSS). The H $\alpha$  detections indicate the presence of cool gas embedded within hotter, X-ray–emitting cluster gas, a signature of a massive cooling flow.

We draw several conclusions about the distant cooling flows revealed by their H $\alpha$  emission. The X-ray and optical properties of these distant cooling flows are similar to cooling flows found nearby ( $z < 0.1$ ). If extended H $\alpha$  emission is an unbiased indicator of a cooling flow (i.e., the relationship between the presence of a cooling flow and detectable H $\alpha$  emission does not change with redshift), then the fraction of X-ray–emitting clusters that possess massive cooling flows has decreased by a factor of about 2 since  $z \sim 0.3$ . The EMSS is rich in distant cooling flow clusters, not because of a selection effect as previously suggested but because cooling flow clusters comprised a large percentage of X-ray–emitting clusters in the past. There is limited evidence that the cosmological evolution of cooling flow clusters may be different from the non-cooling flow clusters.

Also, accounting for the expected differences in the spatial extent of the X-ray emission of cooling flow and non-cooling flow clusters does not alter the conclusion of Gioia et al. that X-ray–luminous clusters have increased in number and/or luminosity since  $z \sim 0.3$ .

One candidate luminous blue arc has been discovered in the course of this study.

*Subject headings:* cooling flows — galaxies: clustering — X-rays: galaxies

### 1. INTRODUCTION

The X-ray–emitting hot gas in the central regions of rich clusters of galaxies is one of the most luminous classes of X-ray emitters in the universe ( $L_x = 10^{43}$ – $10^{46}$  ergs s<sup>-1</sup>; Jones & Forman 1984; Gioia et al. 1990a, hereafter Paper I). Inverted temperature profiles and high densities implying cooling times shorter than a Hubble time for the hot gas and X-ray emission lines from gas that has lost 90% of its thermal energy in some rich clusters (see Canizares, Markert, & Donahue 1988; Fabian, Nulsen, & Canizares 1991) are evidence for nonstatic “cooling flows” in many of these clusters. X-ray–derived mass accretion rates for cooling flows in nearby clusters range from 1 to 1000  $M_\odot$  yr<sup>-1</sup> (e.g., Canizares, Stewart, & Fabian 1983; Stewart et al. 1984; Fabian, Nulsen, & Canizares 1984; Canizares et al. 1979, 1982; Mushotzky et al. 1981). If sustained over a Hubble time, this accretion would result in the accumulation of  $10^{10}$ – $10^{12}$   $M_\odot$ , a significant fraction of the mass of a typical central galaxy. Since persistent cooling flows (CFs) of high  $\dot{M}$  may play a role in the formation of galaxies in the centers of clusters, CF clusters may be common at high redshifts (Fabian et al. 1986). Fabian and Henry and collaborators (e.g., Crawford & Fabian 1989; Henry & Henriksen 1986) have

suggested that the optical and UV emission lines of some quasars and radio galaxies may be powered by CFs.

If the X-ray data are insufficient to reveal whether a cluster contains a CF, it is still possible to discover CFs in X-ray–emitting clusters by searching for optical line emission at the cluster center. In this way the cool gas can be directly detected in hydrogen recombination lines (H $\alpha$ ) or collisionally excited forbidden lines ([O II]  $\lambda 3727$  is the strongest). By obtaining H $\alpha$  narrow-band images of a complete X-ray–selected sample of distant clusters, we seek answers to the following questions: (1) Does a large population of CF clusters exist at high redshifts? (2) Do CFs reside in distant clusters in the same proportions and with the same physical characteristics as CFs in nearby clusters? (3) Do CF clusters evolve in numbers or luminosity with redshift? Also, (4) does the detection of a significant fraction of CFs in a complete sample of clusters alter the assumptions required to derive a luminosity function from that sample (e.g., Paper I) because of the differing spatial distributions of the X-ray emission for CF clusters as compared with non-CF clusters (Pesce et al. 1990)?

Previous studies of H $\alpha$ –emitting filaments in X-ray–emitting clusters, which concentrated on lower redshift ( $z \leq 0.1$ ) clusters (Cowie et al. 1983; Hu, Cowie, & Wang 1985; Heckman 1981; Johnstone, Fabian, & Nulsen 1987; Baum 1987; Baum et al. 1988; Romanishin & Hintzen 1988; Heckman et al. 1989), revealed a correlation between the presence of optically emitting filaments and a CF. Heckman et al. (1989, hereafter HBvM) find a 99.9% correlation between the H $\alpha$  luminosity ( $L_{H\alpha}$ ) and the mass accretion rate ( $\dot{M}_x$ ) determined from X-ray

<sup>1</sup> Visting Astronomer, National Optical Astronomy Observatories (NOAO), Tucson, AZ 85726.

<sup>2</sup> Postal address: The Observatories of the Carnegie Institution of Washington, 813 Santa Barbara Street, Pasadena, CA 91101.

<sup>3</sup> Postal address: Institute for Astronomy, 2680 Woodlawn Drive, Honolulu, HI 96822.

surface brightness data (Arnaud 1988; Sarazin 1986; Fabian, Nulsen, & Canizares 1984; Johnstone, Fabian, & Nulsen 1987; Stewart et al. 1984). Approximately 70% of the brightest cluster galaxies with X-ray–detected CFs have been detected in H $\alpha$  as well (see HBvM, Table 9, for a complete list of the brightest X-ray clusters observed for optical emission lines up to this time). However, the scatter in the relationship between derived  $\dot{M}_x$  and observed  $L_{\text{H}\alpha}$  is large;  $\dot{M}_x \sim 100 M_{\odot} \text{ yr}^{-1}$  can be associated with nebulae of  $L_{\text{H}\alpha} \sim 10^{40.5} - 10^{42.5} \text{ ergs s}^{-1}$ .

Presumably, the H $\alpha$  filaments condense and cool out of the hot gas (Mathews & Bregman 1978; Fabian & Nulsen 1977; Binney & Cowie 1981). These filaments may initially grow from shocked blobs (David, Bregman, & Seab 1988) and then settle down to quasi-steady cooling and accretion (see Meiksin 1990) on longer time scales. The spectra of these filaments indicate that they are probably photoionized by extreme ultraviolet (EUV) radiation emanating from surrounding hotter gas (Voit & Donahue 1990; Donahue & Voit 1991; Begelman & Fabian 1990).

We present the results of an H $\alpha$  imaging survey for a complete X-ray–selected sample of clusters of galaxies drawn from the *Einstein* Extended Medium-Sensitivity Survey (EMSS; Gioia et al. 1990b; Stocke et al. 1991). This H $\alpha$  imaging survey contains clusters more distant ( $0.070 \leq z \leq 0.374$ ) than have been observed before in this manner. Since the presence of H $\alpha$  in X-ray–emitting intracluster gas is empirically correlated with the presence of a CF, we can use the detection of H $\alpha$  to estimate the fraction of clusters with CFs in this sample. We use H $\alpha$  images because we currently lack X-ray imaging with sufficient spatial resolution to resolve a central X-ray excess (e.g., Jones & Forman 1984, hereafter JF1984) or to do deprojection analyses that might reveal the presence of a CF (e.g., Arnaud 1988).

In § 2 we describe the cluster sample, in § 3 the observations and the reduction procedures. In § 4 we report the detections, emission-line fluxes and upper limits, the broad-band colors, and the discovery of a candidate blue arc in the sample. In § 5 we compare the properties of the cluster CFs in this sample with those of a sample of low-redshift cluster CFs. In § 6 we analyze the completeness, selection effects, and flux corrections for the EMSS sample. In § 7 we discuss the evidence for evolution in the sample, and we summarize our results in § 8.

## 2. THE SAMPLE

The 32 clusters selected for this H $\alpha$  imaging survey have been chosen from the EMSS. The EMSS consists of 835 faint ( $7 \times 10^{-14}$  to  $1.5 \times 10^{-11} \text{ ergs cm}^{-2} \text{ s}^{-1}$  in the 0.3–3.5 keV energy band) X-ray sources discovered “serendipitously” at high Galactic latitude ( $|b| \geq -20^\circ$ ) with the imaging proportional counter (IPC). At present more than 96% of these sources are optically identified. The X-ray, optical, and radio properties of this survey are described in detail in Gioia et al. (1990b) and Stocke et al. (1991).

Twenty-three clusters of galaxies observed by us constitute a statistically complete sample of X-ray–selected clusters, in that (1) these are all of the clusters in the EMSS bounded only by  $f_x \geq 8 \times 10^{-13} \text{ ergs cm}^{-2} \text{ s}^{-1}$  and declination  $-20^\circ$  or above, and (2) all of the EMSS sources defined by the above bounds have been optically identified (Stocke et al. 1991). Table 1 lists all of the EMSS clusters observed in this H $\alpha$  survey. A single EMSS cluster (MS 0839.9+2938) has already been reported as a CF cluster (Nesci et al. 1989).

Additional EMSS clusters were also observed which are

fainter in X-rays than the above flux limit, and are denoted with asterisks in Table 1. These clusters were selected either because of the presence of large equivalent width ( $W \geq 25 \text{ \AA}$ ) [O II] 3727  $\text{\AA}$  emission in the optical spectrum of the brightest cluster galaxy or because their total “extended counts” detected by the IPC placed them above the “point-source” flux limit of  $8 \times 10^{-13} \text{ ergs cm}^{-2} \text{ s}^{-1}$  (see below).

The X-ray flux used to define this sample has been computed using the counts in a  $2.4 \times 2.4$  detection cell (the standard for the “REV 1” reprocessing of the IPC data) and then corrected for vignetting, mirror scattering, and point response function. A power-law X-ray spectrum is assumed with an energy index of  $\alpha = -0.5$ , which approximates a Raymond-Smith thermal spectrum for a plasma at a temperature of  $\sim 6 \text{ keV}$ . The neutral hydrogen column density values of Stark et al. (1984) have been used to correct the X-ray flux for Galactic absorption. The “point-source” detection-cell fluxes are given in column (2) of Table 2. The “extended” fluxes, when present, are reported in column (3), as reported in Gioia et al. (1990b).

In Table 2, column (4), we report the X-ray luminosity from within the IPC detection cell, dividing the flux by 1.13 to remove the correction for the point response function, invoking a “K-correction” (of order unity) to calculate the flux in the 0.3–3.5 keV band at the source, and multiply by  $4\pi d_L^2$ , where  $d_L$  is the luminosity distance. We then corrected this luminosity for the extended X-ray flux outside the detection cell as determined from a model of the X-ray surface brightness distribution to obtain the total cluster X-ray luminosity (Table 2, col. [5]). The X-ray surface brightness distribution of the outer region of a cluster atmosphere is well fitted by a King model (also called a  $\beta$ -model in JF1984) in which

$$I(r) = I_0 \left[ 1 + \left( \frac{r}{a_{\text{Mpc}}} \right)^2 \right]^{3\beta - 1/2}, \quad (1)$$

parameterized only by a core size ( $a_{\text{Mpc}}$ ) in megaparsecs and an exponent  $\beta$  which determines the radial variation of the surface brightness distribution. Since JF1984 determined that most X-ray–emitting clusters were well fitted by a  $\beta$ -model with  $\beta = 0.67$  plus a central excess of 0%–30% for CF clusters, the correction for extended X-ray flux is specified straightforwardly by only two parameters,  $a_{\text{Mpc}}$  and a central excess fraction. We correct  $L_x$  for flux outside the detection cell by assuming that the X-ray core radius  $a_{\text{Mpc}}$  is 0.20 and the central excess is 10% for CF clusters, and  $a_{\text{Mpc}} = 0.25$  for non-CF clusters. (See § 6 for the rationale for these choices.)

Because of the uncertainties inherent in the measurement of the extended fluxes, we did not use them to estimate the total cluster luminosity. The reported X-ray fluxes and luminosities are in the 0.3–3.5 keV *Einstein* band (in the rest frame of the observer and the cluster, respectively). We assume  $H_0 = 50 \text{ km s}^{-1}, q_0 = 0.1$  throughout this paper.

### 2.1. Distinction between Extended and Point-Source Counts

The precise manner in which the EMSS clusters were selected must be carefully defined, because the selection method could lead to a bias in the type of clusters which appear in our sample. Distant cluster X-ray emission can be spatially extended on an angular scale of a few arcminutes, but detection by the IPC REV 1 algorithm is based upon excess counts in a single detection cell; thus a detection is made on the basis of the central or peak surface brightness or an extended source, not the total flux of the source. This type of bias, is, of course,

TABLE 1  
OBSERVING LOG

Cluster Name	Redshift	Dates (UT)	Filters (KPNO)	$t_{\text{exp}}$ (s)	Photometric?
MS 0002.8+1556	0.116	1988 Oct 17	7336	2400	N
MS 0011.7+0837	0.163	1988 Oct 14	7630	2400	Y
MS 0026.4+0725*	0.170	1988 Oct 16	7680	2400	N
MS 0037.8+2917 (A77)	0.069	1988 Oct 14	7007	2400	N
MS 0102.3+3255	0.080	1988 Oct 16	7099	1800	N
MS 0109.4+3910*	0.208	1988 Oct 15	7935	3000	N
MS 0433.9+0957	0.159	1988 Oct 15–16	7630	2400	N
MS 0440.5+0204	0.190	1988 Oct 14	7832	2400	N
MS 0451.5+0250 (A520)	0.202	1989 Mar 6	7883	2400	Y
MS 0735.6+7421	0.216	1988 Oct 14	958	2400	Y?
MS 0839.8+2938	0.194	1988 Oct 14	7832	2400	Y?
MS 0849.7–0521*	0.192	1988 Oct 16	7730	2400	N
MS 0904.5+1651 (A744)*	0.073	1989 Mar 5, 8	7053	2400	Y
MS 0906.5+1110	0.180	1989 Mar 6	7730	2400	Y
MS 1006.0+1202	0.221	1989 Mar 6	958	3600	Y
MS 1008.1–1224*	0.301	1989 Mar 6	116	3600	Y
MS 1050.7+4946	0.140	1989 Mar 5, 8	7482	2400	Y
MS 1127.7–1418 (A1285)	0.105	1989 Mar 6	7240	1847	Y
MS 1224.7+2007*	0.327	1989 Mar 8	35-4530 <sup>a</sup>	6000	Y
MS 1244.2+7114	0.225	1989 Mar 5	958	3600	Y
MS 1306.7–0121	0.088	1989 Mar 5	7146	2400	Y
MS 1358.4+6245	0.328	1989 Mar 6–7	35-4530 <sup>a</sup>	3600	Y
MS 1426.4+0158*	0.320	1989 Mar 7–8	35-4530 <sup>a</sup>	6000	Y
MS 1455.0+2232	0.258	1989 Mar 6	35-4456 <sup>a</sup>	3600	Y
MS 1512.4+3647*	0.374	1989 Mar 8	673 <sup>b</sup>	3600	Y
MS 1522.0+3003 (A2069)	0.116	1989 Mar 7	7336	2400	Y
MS 1531.2+3118 (A2092)*	0.067	1989 Mar 7	7007	1800	Y
MS 1558.5+3321 (A2145)	0.088	1989 Mar 5, 8	7146	2400	Y
MS 1754.9+6803	0.077	1989 Mar 5–6	7053	1800	Y
MS 1910.5+6736	0.246	1988 Oct 16–17	988	3600	N
MS 2216–0401	0.090	1988 Oct 14	7193	2400	Y
MS 2348.0+2913	0.095	1988 Oct 14	7193	2400	Y

NOTE.—Clusters marked with asterisks are not part of the X-ray flux-limited sample.

<sup>a</sup> Ealing filter number.

<sup>b</sup> [O II] filter.

not unique to X-ray astronomy, since it may play an important role in optical counts of galaxies (e.g., Sandage, Binggeli, & Tammann 1985; Impey, Bothun, & Malin 1988; Bothun 1986), based on the discovery of very low surface brightness galaxies with large total fluxes (e.g., Malin 1; Bothun et al. 1987).

In the context of X-ray-emitting clusters, this section effect has been discussed in detail by Pesce et al. (1990), who suggested that most or all distant clusters found within the EMSS (and other X-ray imaging surveys; e.g., *ROSAT* all-sky survey) would be CF clusters because of this manner of selection. That is, selecting X-ray-emitting clusters by their peak surface brightness rather than total flux biases the type of cluster detected in favor of those clusters which are more compact spatially. (A cluster sample could be chosen for total flux using an instrument with poorer spatial resolution but the same sensitivity as the IPC, but such a sample could contain source confusion errors.) Because the extended X-ray emission seen in nearby CFs often has a sharp central peak (Arnaud 1988 or JF1984), CF clusters generally have a higher peak surface brightness than non-CF clusters with the same total X-ray flux. We agree with the Pesce et al. analysis in principle, but suspect that this selection bias is not as great as they suggest (see § 6).

The EMSS sample studied herein provides an example of the operation of this selection bias. In Table 2, column (3), we list fluxes for all of the bright EMSS clusters for which counts were detected in more than one detection cell by the REV 1 repro-

cessing (so-called extended counts). Many of these are already in our flux-limited sample, but six have point-source fluxes below the limit of  $8 \times 10^{-13}$  ergs  $\text{cm}^{-2}$   $\text{s}^{-1}$  that we set for inclusion in our complete sample. If the IPC spatial resolution were a factor of 2–3 times poorer (and thus the detection cell optimal for point-source detection were larger), these sources would have larger X-ray fluxes than those listed in Table 2 and would have been included in our sample. Perhaps there are other clusters of very low surface brightness but of high total flux that the IPC detection algorithm does not detect at all (the X-ray analog of the very low surface brightness spiral galaxies) but which, nonetheless, have total X-ray fluxes in excess of our flux limit.

All of the clusters marked with an asterisk and with extended counts in Table 2 were observed by us in this H $\alpha$  imaging program (except MS 1621.5+2640),<sup>4</sup> and none were detected in H $\alpha$ . Clearly, the exclusion of these objects from our complete sample alters the statistics of CFs within the sample as a whole. Because this point bears on the analysis of our complete sample data, we present a detailed discussion and modeling of this effect in § 6.

<sup>4</sup> MS 1621.5+2640 has only recently been identified as a distant cluster of galaxies and is at such high redshift ( $z = 0.426$ ) that no H $\alpha$  filter was available at the correct wavelength; thus no H $\alpha$  imaging observations have been made of this cluster.

TABLE 2  
X-RAY MEASUREMENTS

Cluster Name (1)	$F_x$ (Detection Cell) ( $\times 10^{-13}$ ) (2)	$F_x$ (Extended) ( $\times 10^{-13}$ ) (3)	$L_x$ (Detection Cell) ( $\times 10^{44}h_{50}^{-2}$ ergs $s^{-1}$ ) (4)	$L_x$ (Corrected) ( $\times 10^{44}h_{50}^{-2}$ ergs $s^{-1}$ ) (5)
MS 0002.8 + 1556 .....	8.23	20.16	0.441	1.68
MS 0011.7 + 0837 .....	13.11	13.11	1.413	3.90
MS 0026.4 + 0725* .....	5.32	5.32	0.625	1.22
MS 0037.8 + 2917 .....	21.06	69.98	0.392	2.86
MS 0102.3 + 3255 .....	8.75	8.75	0.220	0.713
MS 0109.4 + 3910* .....	2.10	5.39	0.375	0.865
MS 0433.9 + 0957 .....	15.53	15.53	1.59	4.48
MS 0440.5 + 0204 .....	11.51	11.51	1.70	3.14
MS 0451.5 + 0250 .....	18.48	72.74	3.11	7.31
MS 0735.6 + 7421 .....	14.80	42.93	2.85	4.97
MS 0839.8 + 2938 .....	14.95	23.31	2.31	4.21
MS 0849.7 - 0521* .....	3.34	12.34	0.505	1.23
MS 0904.5 + 1651* .....	6.58	13.94	0.137	0.926
MS 0906.5 + 1110 .....	17.76	30.63	2.35	6.00
MS 1006.0 + 1202 .....	11.29	22.63	2.29	3.94
MS 1008.1 - 1224* .....	6.66	14.70	2.58	4.87
MS 1050.7 + 4946 .....	14.09	14.09	1.11	2.41
MS 1127.7 - 1418 .....	15.28	73.65	0.668	2.83
MS 1224.7 + 2007* .....	5.99	5.99	2.76	4.17
MS 1244.2 + 7114 .....	8.78	8.78	1.85	3.16
MS 1306.7 - 0121 .....	10.74	26.45	0.328	1.72
MS 1358.4 + 6245 .....	13.82	13.82	6.42	9.68
MS 1426.4 + 0158* .....	4.99	8.00	2.20	4.04
MS 1455.0 + 2232 .....	29.88	29.88	8.43	13.7
MS 1512.4 + 3647* .....	5.07	5.07	3.08	4.49
MS 1522.0 + 3003 .....	11.76	84.28	0.631	2.39
MS 1531.2 + 3118* .....	3.36	15.68	0.060	0.449
MS 1558.5 + 3321 .....	8.98	20.17	0.274	1.44
MS 1754.9 + 6803 .....	10.17	10.17	0.237	0.79
MS 1910.5 + 6736 .....	8.82	8.82	2.23	4.66
MS 2216 - 0401 .....	19.47	70.92	0.622	3.17
MS 2348.0 + 2913 .....	16.63	16.63	0.593	1.67

NOTE.—Clusters marked with asterisks are not part of the X-ray flux-limited sample.

## 2.2. Cooling Flow Galaxies

After the imaging program was begun, two X-ray sources were deleted from the complete sample discussed here because there was no rich cluster present. MS 1019.0 + 5139 and MS 1826.5 + 7256 have low-ionization, optical emission-line spectra ( $[\text{O II}] \lambda 3727 \gg [\text{O III}] \lambda 5007$ ; see Stocke et al. 1991) identical to that displayed by the central galaxies in cooling flow clusters, but no surrounding rich cluster is present. These two sources and three others are the only EMSS sources identified with a new class of faint X-ray emitters, which we term “cooling flow” galaxies. These sources will be discussed in detail in a separate publication (Stocke et al. 1992).

## 3. OBSERVATIONS AND REDUCTIONS

We observed the 32 EMSS clusters in Table 1 on UT 1988 October 13–17 and 1989 March 5–8 with Kitt Peak National Observatory (KPNO) 2.1 m telescope plus direct camera with the Tek 1 CCD. For each cluster field, we took Gunn *R* and Mould *B* broad-band images of 5–7 minutes length and redshifted  $\text{H}\alpha$  images of 30–80 minutes duration. The  $\text{H}\alpha$  images were obtained primarily by utilizing the KPNO  $\text{H}\alpha$  *B* filter set ( $\Delta\lambda \sim 75 \text{ \AA}$  and transmission  $\sim 80\%$ ), but other narrow-band filters ( $\Delta\lambda \sim 100 \text{ \AA}$ ) with peak transmission percentages of 50%–70% were also used when necessary ( $z \gtrsim 0.2$ ). Most of the additional filters we used were taken from Kitt Peak’s extensive filter collection and are denoted in Table 1 by their KPNO numbers, but two additional filters were used: (1) Ealing

35-4530 is a filter with a central wavelength  $\lambda_c$  of 8708  $\text{\AA}$ ,  $\Delta\lambda \sim 128 \text{ \AA}$ , and peak transmission of 49%; (2) Ealing filter 35-4456 with  $\lambda_c = 8310 \text{ \AA}$ , and  $\Delta\lambda = 108 \text{ \AA}$ , and peak transmission of 59.5%. In one instance (MS 1512.4 + 3647) an image was taken at redshifted  $[\text{O II}]$  owing to the lack of an appropriate filter for  $\text{H}\alpha$ . In the fall, only a few of the exposures were made under completely photometric conditions. High thin clouds were present during most of the observations. In two of the fall observations the humidity was high, but the sky appeared to be cloudless (marked in Table 1 in the “Photometric?” column as “Y?”). In the spring, all of the exposures were made during photometric conditions.

Data were bias-subtracted and flat-fielded with dome flats using the standard IRAF and telescope data reduction packages. Some of the high-redshift fields were fringe-corrected by using sky flats created by median filtering all fields observed with the same filter to remove sources. These flats were scaled and subtracted from the source fields to remove the fringes. For all targets we scaled the red images using the companion galaxies in the cluster as standard and subtracted the scaled images from the  $\text{H}\alpha$  images to make the companion cluster galaxies “disappear.” Since the colors of elliptical galaxies and the underlying stellar population of cD galaxies are similar, this technique effectively subtracts the underlying stellar continuum from the central galaxy. The on-band, off-band subtraction procedure also removed much of the fringing evident in some of the dome-flattened  $\text{H}\alpha$  images.

We calibrated the fluxes by observing the standard star Hiltner 600 (Stone 1977) through most of our filters, and then used filter and chip quantum efficiencies to predict count rates through the remaining filters. Since Hiltner 600 and the clusters were observed through very similar air masses and at very red wavelengths, no correction was included (typical correction  $\sim 3\%$ ) for differential air-mass extinction.

#### 4. RESULTS

##### 4.1. Detections and Fluxes

We detected optical line emission at the  $5\sigma$  level in nine out of 23 clusters in the complete X-ray flux-limited sample. Two additional detections were made at the  $3\sigma$  to  $4\sigma$  level. In Table 3 we present our results for the  $H\alpha + [N II]$  (and one  $[O II]$ ) detections and  $3\sigma$  errors and upper limits within 10 kpc of the central galaxy. For each detection we report the average diameter of the emission region. The upper limits and fluxes may be somewhat underestimated for those few images noted in Table 1 with a "N" or "Y?" in the photometric column. We are confident that our detections are real even in frames contaminated by fringing due to OH night-sky emission lines because the fringing has a larger spatial scale than the emission from the galaxy. In these cases, the error in the flux estimate for these high-redshift clusters is increased by  $\sim 10\%$  of the total

emission-line flux due to the additional manipulation of the data required to flatten the sky completely.

The upper limits and errors in Table 3 were derived formally by assuming Poisson statistics (since the Tek 1 CCD has very low read noise, the exposures are sky-limited) in the CCD electrons for the  $H\alpha$  and red images and by accounting for the error in the ratio we used to subtract the continuum red light from the  $H\alpha$  image. The uncertainty in the ratio dominates the total error. We estimate this uncertainty by measuring the fluxes of several different comparison galaxies in the same cluster, deriving flux ratios for each individual galaxy, and empirically estimating the uncertainty in the ratio used by comparing the ratios for different galaxies in the same image. In most cases, the relative uncertainty of the ratio was of the order of a few percent. If no source was detected, we measured the  $3\sigma$  limit for  $H\alpha$  within 10 kpc of the center of the galaxy.

According to our error analysis, we can be confident that we have detected  $H\alpha$  flux to a limit of  $(1-5) \times 10^{-15}$  ergs  $s^{-1}$   $cm^{-2}$  over the area of sky subtended by the central 10 kpc of the dominant galaxy in each of the X-ray clusters. This corresponds to luminosities of  $(4.7-23.0) \times 10^{40}$  ergs  $s^{-1}$  ( $z = 0.1$ ) and  $(9.5-48) \times 10^{41}$  ergs  $s^{-1}$  ( $z = 0.4$ ).

In Figures 1-4 (Plates 1-4), we present images and contour plots of all of the  $H\alpha$  detections, including the clusters not in the flux-limited sample. The gray-scale image was taken through the Gunn  $R$  filter, and the contour plot is of the net  $H\alpha + [N II]$  image, with contours at listed levels. The first contour is approximately at the  $3\sigma$  level of the noise in the image. In Figures 1-4 we have indicated that some subtracted images were boxcar-smoothed (size listed in caption) in order to reduce the noise in the background and produce a continuous contour plot. No Galactic reddening is included in reporting the surface brightness levels. Foreground stars in these images may also appear to have slight  $H\alpha$  emission because they may be significantly bluer than the stellar continuum of the underlying cluster galaxy. Some images contain remnants of bad columns due to chip defects in the CCD (noted in plate legends).

For  $H\alpha + [N II]$  luminosities we computed the Galactic reddening correction at redshifted  $H\alpha$  assuming that  $\tau \approx 0.4(N_H/10^{21} \text{ cm}^{-2})(1+z)^{-1}$  (Draine & Lee 1984). This correction, based on H I column densities from Stark et al. (1984), ranges from 4% to 60%, with a median of about 10%. Only one cluster has an estimated reddening correction greater than 30% due to high Galactic column density: MS 0433.9+0957 with an H I column of  $1.4 \times 10^{21} \text{ cm}^2$ . We report the  $H\alpha$  and  $[N II]$  line luminosities and average emission diameters in Table 3.

The six observations which are possibly nonphotometric do not affect our analysis, since these observations essentially were randomly selected out of the sample. Also, since the percentage of non-photometric observations that resulted in detections is the same percentage detected in the photometric subsample, there is no overall counting bias introduced by including the non-photometric observations. Therefore, all subsequent analyses include these observations.

##### 4.2. Broad-Band Colors and Blue Arcs

A preliminary analysis did not reveal an unusual number of blue objects in the fields. Based upon subsequent spectroscopy, the blue objects in the frames were generally foreground galaxies. In other words, scaling the red image and subtracting it from the blue image removes almost all of the galaxies in the

TABLE 3  
 $H\alpha + [N II]$  MEASUREMENTS

Cluster Name	$H\alpha + [N II]$ Flux ( $\times 10^{-15}$ )	$L_{H\alpha+[N II]}$ ( $\times 10^{40}$ ergs $s^{-1}$ )	Scale D (kpc)
MS 0002.8+1556 .....	<1.0	<5.6	...
MS 0011.7+0837 .....	<2.5	<27	...
MS 0026.4+0725* .....	$1.2 \pm 0.4$	$15 \pm 5$	12.5
	$2.0 \pm 0.4$	$25 \pm 5$	12.5
	<3.4	<5.4	...
MS 0037.8+2917 .....	$3.3 \pm 1$	$8.0 \pm 3.6$	6.7
MS 0102.3+3255 .....	<1.0	<19	...
MS 0109.4+3910* .....	<1.0	<19	...
MS 0433.9+0957 .....	<6	<46	...
MS 0440.5+0204 .....	$12 \pm 2.6$	$160 \pm 30$	33
MS 0451.5+0250 .....	<0.9	<15	...
MS 0735.6+7421 .....	$9 \pm 2.0$	$190 \pm 40$	32
MS 0839.8+2938 .....	$6 \pm 0.8$	$100 \pm 10$	19
MS 0849.7-0521* .....	<2.6	<38	...
MS 0904.5+1651* .....	<5	<11	...
MS 0906.5+1110 .....	<0.87	<12	...
MS 1006.0+1202 .....	$2.3 \pm 0.9$	$50 \pm 20$	24
MS 1008.1-1224* .....	<0.67	<28	...
MS 1050.7+4946 .....	$1.0 \pm 1.5$	$9 \pm 14$	9.6
MS 1127.7-1418 .....	<1.9	<8.6	...
MS 1224.7+2007* .....	$2.7 \pm 0.5$	$150 \pm 30$	18
MS 1244.2+7114 .....	$12.8 \pm 2.6$	$320 \pm 70$	...
MS 1306.7-0121 .....	<2	<6.7	...
MS 1358.4+6245 .....	$3.6 \pm 0.8$	$200 \pm 45$	24
MS 1264.4+0158* .....	<0.76	<40	...
MS 1455.0+2232 .....	$29 \pm 4$	$930 \pm 130$	45.3
MS 1512.4+3647* .....	$0.58 \pm 0.24^a$	$45 \pm 19$	19
MS 1522.0+3003 .....	<1.0	<6.9	...
MS 1531.2+3118* .....	<3.0	<6.5	...
MS 1558.5+3321 .....	<6.5	<20	...
MS 1754.9+6803 .....	$2.0 \pm 1.5$	$4.6 \pm 3.4$	5
MS 1910.5+6736 .....	<0.9	<24	...
MS 2216-0401 <sup>b</sup> .....	<4	<14	...
MS 2348.0+2913 .....	$2.6 \pm 2.4$	$9.1 \pm 8.4$	18

NOTE.—Clusters marked with asterisks are not part of the X-ray flux-limited sample.

<sup>a</sup>  $[O II]$  emission.

<sup>b</sup> Two separate EMSS detections; only one cluster.

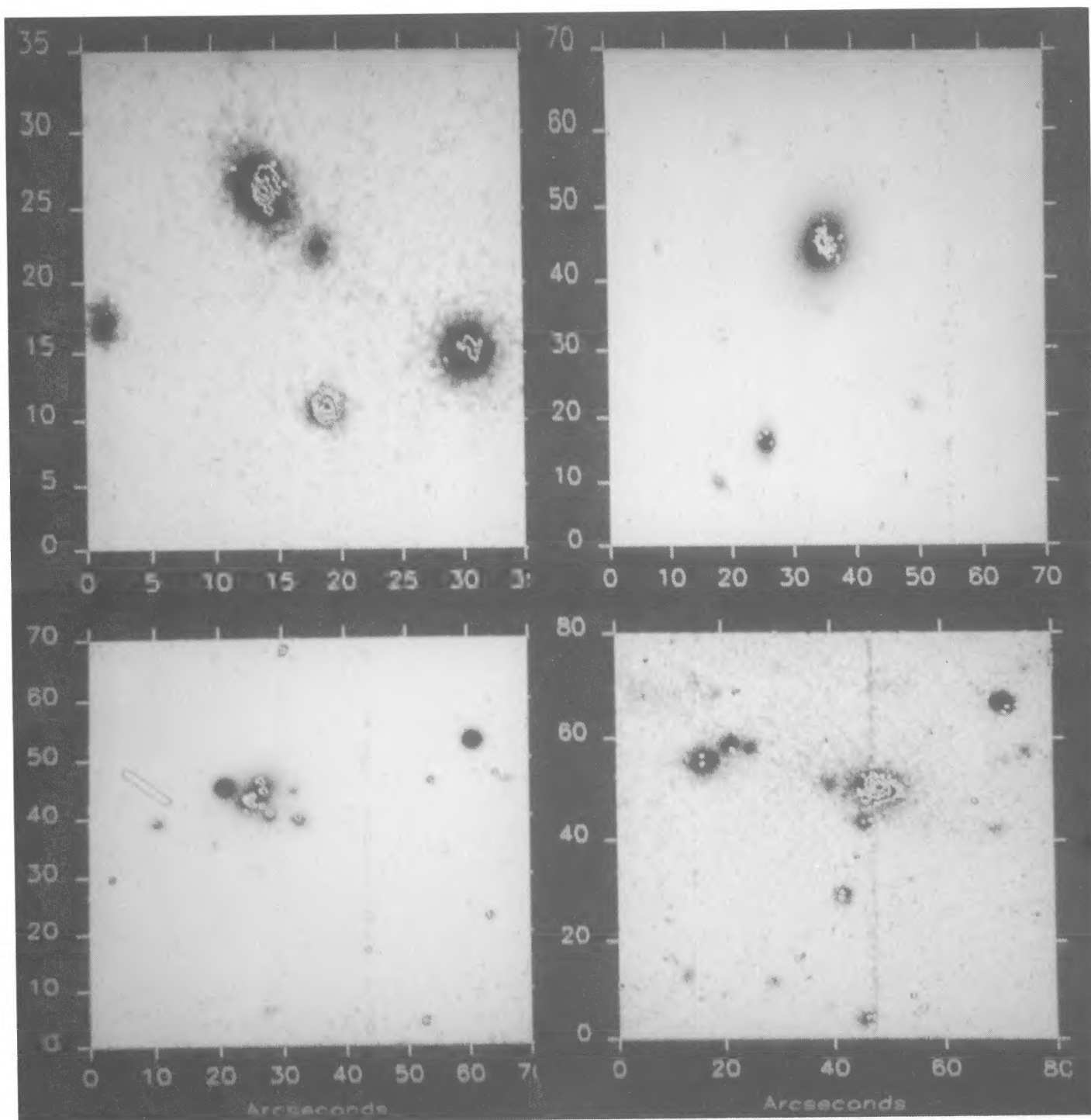


FIG. 1.—Contour plots of continuum- and sky-subtracted images of H $\alpha$  and [N II] emission overlaid on the Gunn  $R$  image, with the first contour at the  $\sim 3\sigma$  noise level. When necessary, we smoothed the differenced image with a boxcar algorithm of indicated size in order to plot the contours continuously. North is to the top of the page, and east is to the right in all pictures in this paper; the field of view in arcseconds is indicated on an axis labeling the western border of each frame. *Top left*: MS 0026.4+0725 (not in the complete sample). Contour levels are  $(1.27, 2.54, 3.81, 6.35, 7.62) \times 10^{-16}$  ergs cm $^{-2}$  s $^{-1}$  arcsec $^{-2}$ . *Top right*: MS 0102.3+3255. Contour levels are  $(1.95, 4.54, 7.14) \times 10^{-16}$  ergs cm $^{-2}$  s $^{-1}$  arcsec $^{-2}$ . A bad CCD column is noted to the north of the galaxy. *Bottom left*: MS 0440.5+0250. We used a  $0''.8 \times 0''.8$  boxcar smoothing procedure. Contour levels are  $(1.16, 1.89, 2.61) \times 10^{-16}$  ergs cm $^{-2}$  s $^{-1}$  arcsec $^{-2}$ . A bad CCD column is to the north, and a cosmic-ray streak is to the south. *Bottom right*: MS 0735.6+7421. Contour levels are  $(1.33, 3.56, 5.79) \times 10^{-16}$  ergs cm $^{-2}$  s $^{-1}$  arcsec $^{-2}$ . A bad CCD column runs through the galaxy, but does not affect the detection significance.

DONAHUE, STOCKE, & GIOIA (see 385, 53)

## PLATE 2

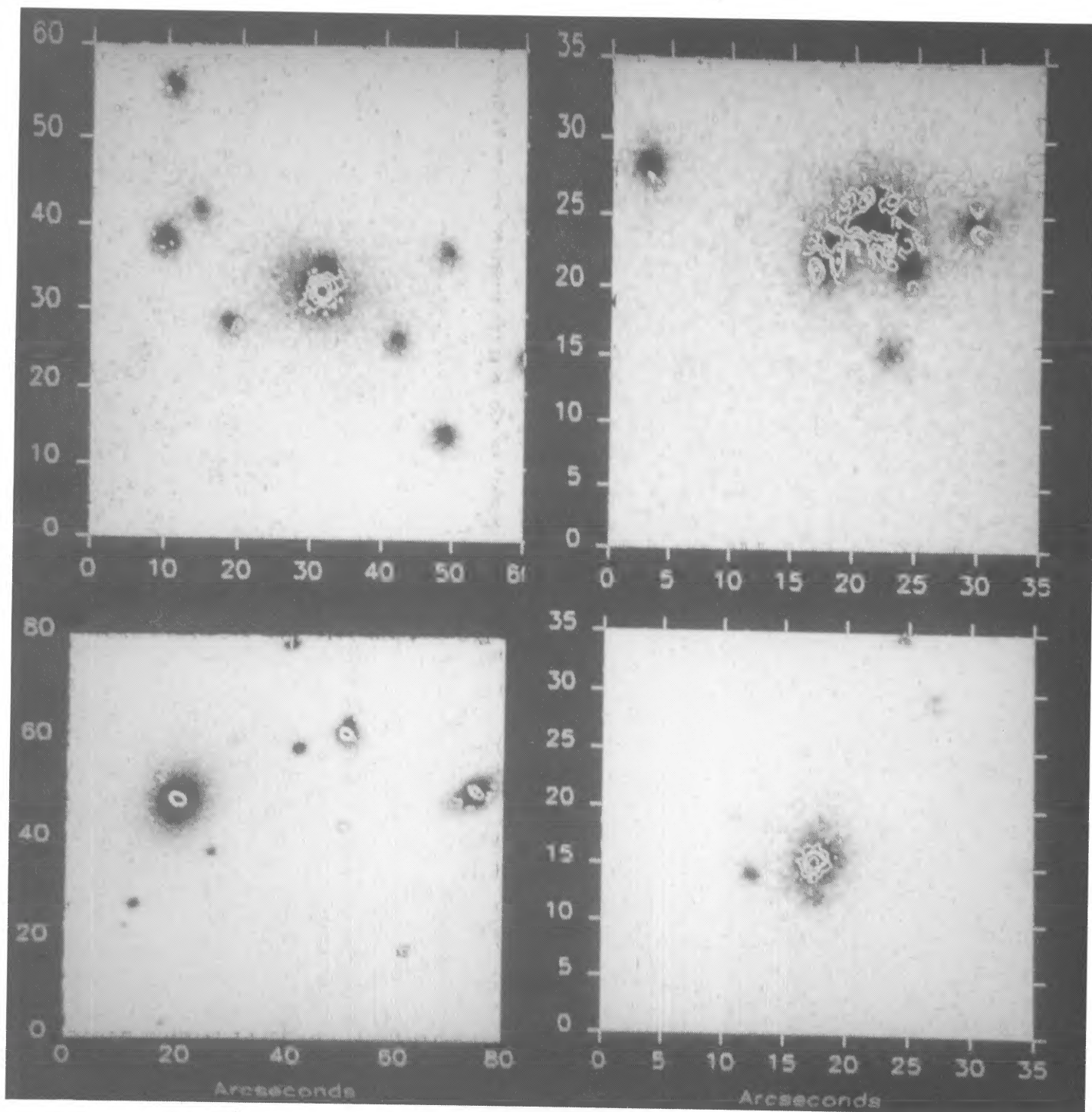


FIG. 2.—Similar to Fig. 1. *Top left*: MS 0339.8 + 2938. Contour levels are  $(1.45, 3.63, 5.81, 7.99) \times 10^{-16} \text{ ergs cm}^{-2} \text{ s}^{-1} \text{ arcsec}^{-2}$ . A bad CCD column is noted to the north. *Top right*: MS 1006.0 + 1202. Contour levels are  $(0.89, 1.19, 1.48) \times 10^{-16} \text{ ergs cm}^{-2} \text{ s}^{-1} \text{ arcsec}^{-2}$ . We used a  $0''.93 \times 0''.93$  boxcar smoothing procedure. *Bottom left*: MS 1050.7 + 4946. Contour levels are  $(0.50, 1.01, 1.51) \times 10^{-16} \text{ ergs cm}^{-2} \text{ s}^{-1} \text{ arcsec}^{-2}$ . Only a  $3\sigma$  detection. We used a  $1''.61 \times 1''.61$  boxcar smoothing procedure. *Bottom right*: MS 1224.7 + 2007. (Not in complete sample.) Contour levels are  $(1.18, 3.54, 5.90, 11.80) \times 10^{-16} \text{ ergs cm}^{-2} \text{ s}^{-1} \text{ arcsec}^{-2}$ .

DONAHUE, STOCKE, & GIOIA (see 385, 53)

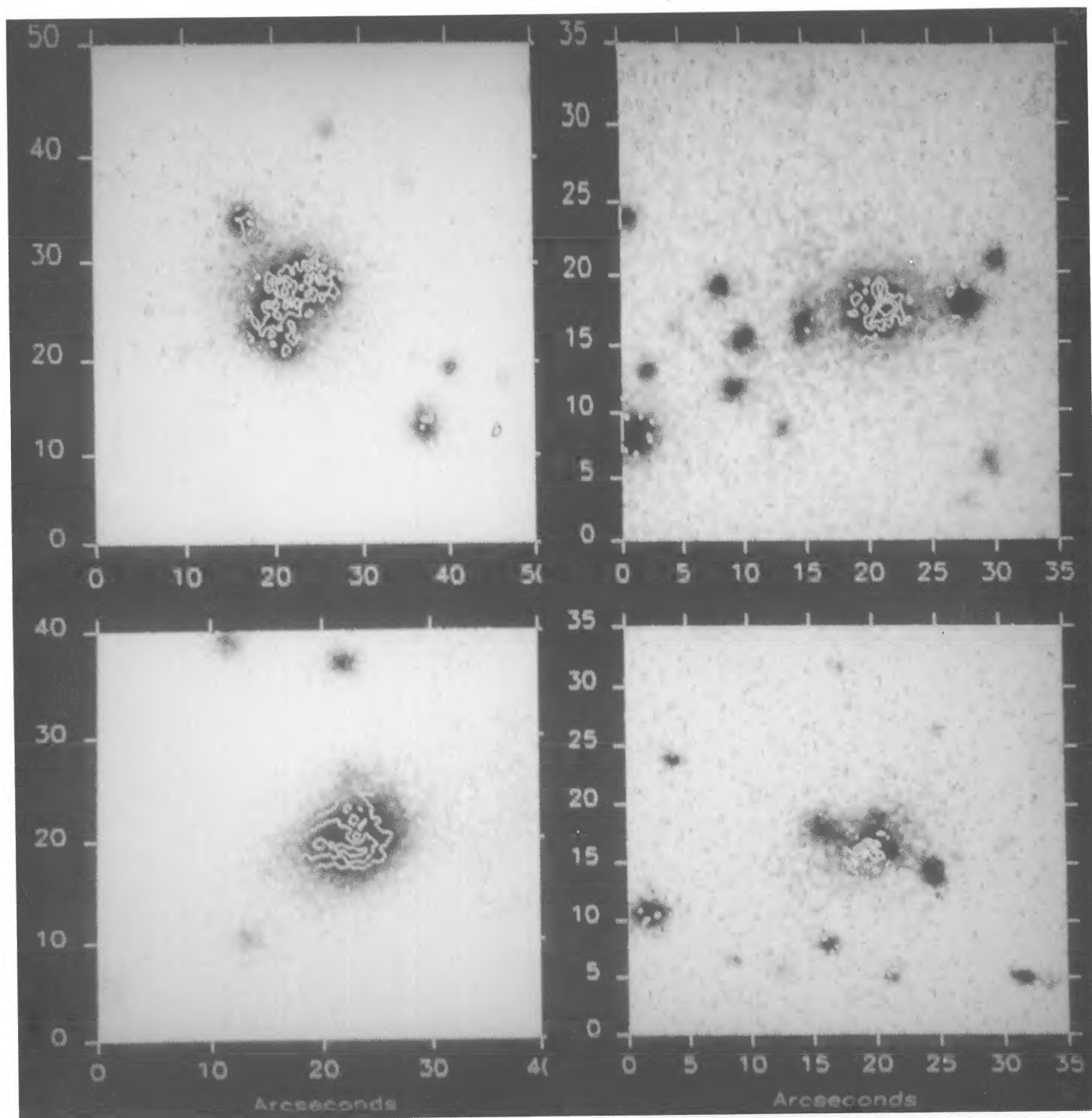


FIG. 3.—Similar to Fig. 1. *Top left*: MS 1244.2+7114. Contour levels are  $(0.58, 0.87, 1.16) \times 10^{-16}$  ergs  $\text{cm}^{-2} \text{s}^{-1} \text{arcsec}^{-2}$ . We used a  $1''.19 \times 1''.19$  boxcar smoothing procedure. *Top right*: MS 1358.4+6245. Contour levels are  $(1.48, 4.43, 7.38) \times 10^{-16}$  ergs  $\text{cm}^{-2} \text{s}^{-1} \text{arcsec}^{-2}$ . *Bottom left*: MS 1455.0+2232. Contour levels are  $(0.78, 1.36, 1.95) \times 10^{-16}$  ergs  $\text{cm}^{-2} \text{s}^{-1} \text{arcsec}^{-2}$ . We used a  $0''.5 \times 0''.5$  boxcar smoothing procedure. *Bottom right*: MS 1512.4+3118. (Not in the complete sample.) Contour levels are  $(0.54, 1.07, 1.61) \times 10^{-16}$  ergs  $\text{cm}^{-2} \text{s}^{-1} \text{arcsec}^{-2}$ . The emission seen here is  $[\text{O II}] \lambda 3727$ .

DONAHUE, STOCKE, & GIOIA (see 385, 53)

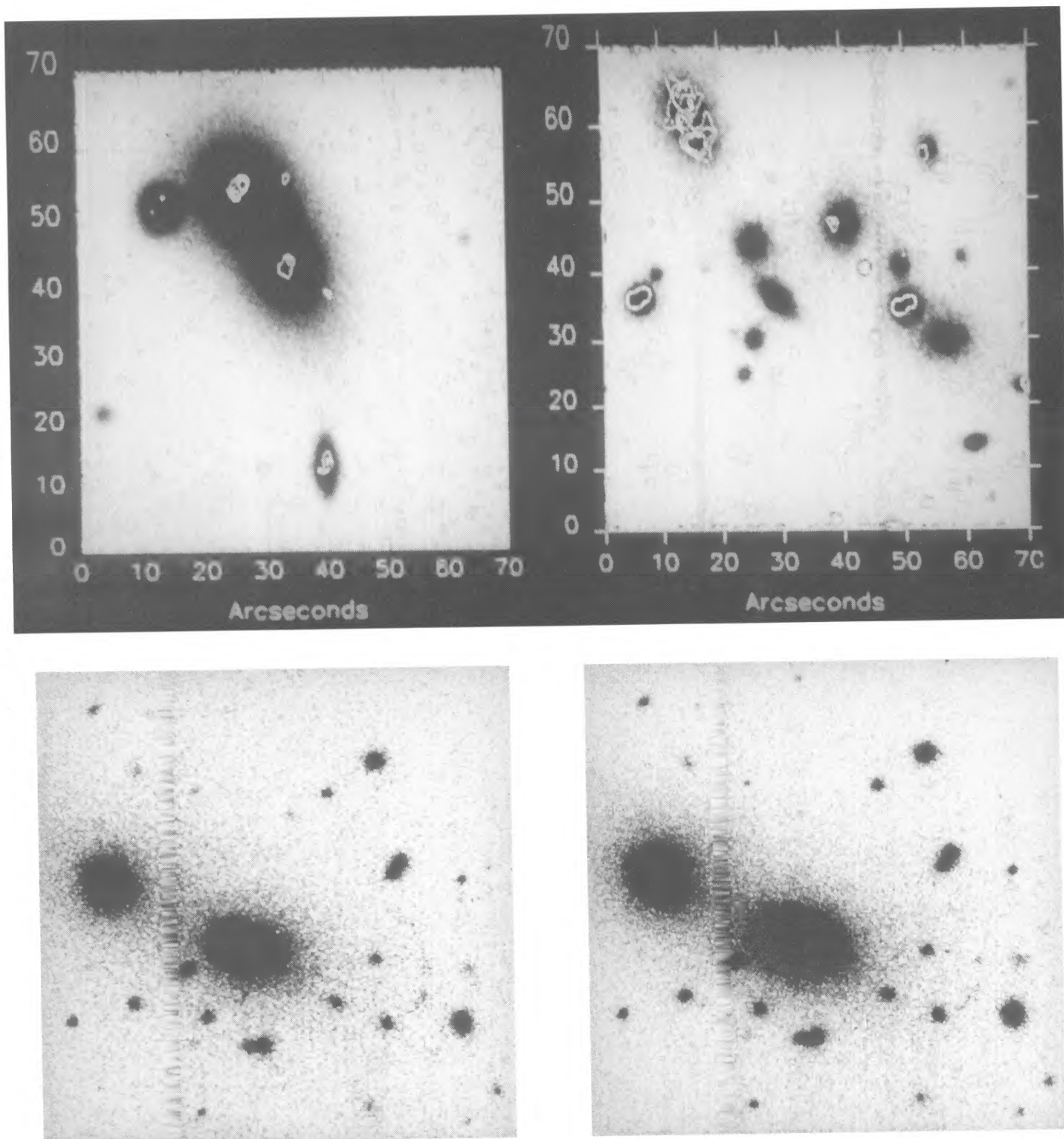


FIG. 4.—Similar to Fig. 1. *Top left*: MS 1754.9+6803. Contour levels are  $(0.87, 2.50, 4.12) \times 10^{-16} \text{ ergs cm}^{-2} \text{ s}^{-1} \text{ arcsec}^{-1}$ . This source may not be extended. *Top right*: MS 2348.0+2913. Contour levels are  $(0.34, 0.55, 0.75) \times 10^{-16} \text{ ergs cm}^{-2} \text{ s}^{-1} \text{ arcsec}^{-2}$ . We used a  $1''.78 \times 1''.78$  boxcar smoothing procedure. *Bottom left*: East is at the top, and north is to the left. The fields of view are  $1''.4 \times 1''.4$ . A Mould B image showing the blue arc feature to the south (right) of the largest galaxy in the cluster MS 1522.0+3004. The average surface brightness of this feature is  $\sim 21 \text{ B mag arcsec}^{-2}$ . *Bottom right*: East is at the top, and north is to the left. Gunn R filter image of MS 1522.0+3004 to use as a comparison for the Mould B image. This image shows little or no evidence for the arc candidate showing in the blue image, which indicates that the arc is fairly blue.

DONAHUE, STOCKE, & GIOIA (see 385, 53)

blue image. We also note no change with cluster redshift in the fraction of galaxies which are not completely removed by subtraction. We did not do a careful Butcher-Oemler analysis (e.g., Butcher & Oemler 1984), however, owing to the limitations of our data (i.e., the poor blue sensitivity of the Tek 1 CCD chip and the low exposure levels of companion galaxies, which made it difficult to establish a comparison ratio with very high statistical significance). Only five bright galaxies have blue images that would be uncontaminated by [O II] emission in the Mould *B* filter. There does not seem to be any evidence for the presence of excess blue light, such as that from young stars, in these galaxies. In Butcher & Oemler's (1984) careful reanalysis of this effect in clusters with  $z \leq 0.5$ , they report that even clusters which are very luminous in X-rays, such as 3C 295, have an excess of blue galaxies as compared with nearby field or cluster galaxies. A deeper blue color survey of an X-ray-selected sample of clusters such as the EMSS clusters, with redshifts to confirm cluster membership, is warranted to investigate the Butcher-Oemler effect in this sample.

A blue arc candidate was discovered at the level of  $20.9 \pm 0.3$  mag arcsec<sup>-2</sup> in the broad-band Mould *B* images in MS 1522.0+3003 (A2069). We show this detection in the last two panels of Figure 4. This single detection in a sample of 32 clusters is consistent with an estimate (J. A. Tyson 1990, private communication) that approximately one in 20 X-ray clusters have a bright arc. Because it is bright, spectroscopy of this arc should determine whether it is a galaxy being lensed by MS 1522.0+3003.

##### 5. COMPARISON WITH LOW-REDSHIFT COOLING FLOWS

To compare the optical properties of nearby and distant cooling flows, we use a sample of 37 nearby clusters listed in HBvM which have been examined for optical line emission by various observers. These clusters are, in general, the brightest clusters with H $\alpha$  data, but the sample is somewhat heterogeneous. However, we regard the optical properties of clusters in this sample as representative of those of nearby cooling flows, since these clusters were selected for optical observation on the basis of their X-ray luminosities and  $\dot{M}_x$  and not for their optical properties. We will use this comparison sample to describe qualitatively the characteristic optical and X-ray features of clusters of galaxies with cooling flows, and to estimate the fraction of cooling flows with H $\alpha$  emission.

Since most but not all CFs have luminous H $\alpha$  emission, in order to estimate how many CFs exist in the EMSS sample, we need an estimate of how many CFs we do not identify because of the weakness of their H $\alpha$  emission. Thirty-one of the 37 HBvM clusters have X-ray-determined  $\dot{M}$ , and, of these, nine (~30%) have only upper limits on their H $\alpha$  emission of  $(0.26-5.3) \times 10^{41} h_{75}^2$  ergs s<sup>-1</sup>, where  $h_{75} = H_0/75$  km s<sup>-1</sup>; the others are detected well in excess of these limits. Some of these CFs with H $\alpha$  upper limits are quite massive, e.g., A978 and A2029 with  $\dot{M} \sim 222$  and  $156 M_\odot$  yr<sup>-1</sup>, respectively, based upon analysis of their X-ray emission (Arnaud 1988). Thus, ~70% of CFs also emit optical lines. Therefore, if we could detect H $\alpha$  at the luminosity levels listed in HBvM, we would expect to detect ~70% of the CFs in the EMSS sample. However, our sample of clusters is more distant than almost all of those listed in HBvM; thus we would (conservatively) be able to detect only the brightest 32% of the CFs listed in HBvM according to the H $\alpha$  detection limits  $[(1-5) \times 10^{-15}$  ergs s<sup>-1</sup> cm<sup>-2</sup>] of our optical survey. Having detected H $\alpha$  in 39% of the EMSS clusters that we have observed, we cannot

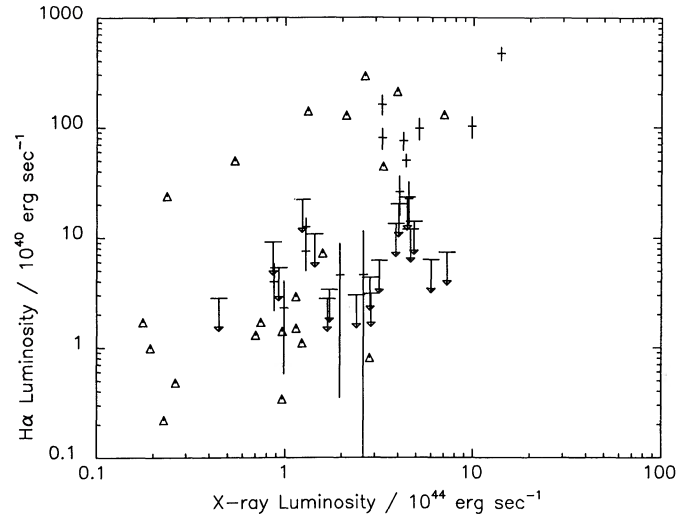


FIG. 5.— $L_x(0.3-3.5$  keV) vs.  $L_{H\alpha}$ .  $H_0 = 50$  km s<sup>-1</sup> Mpc<sup>-1</sup>,  $q_0 = 0.1$ , and  $H\alpha/[N II] \sim 1$  are assumed. Values of  $L_x$  for EMSS clusters are corrected for flux lost outside the detection cell (see text). Errors and upper limits are  $3\sigma$ . The H $\alpha$  upper limits were derived within a radius of 10 kpc at the dominant galaxy in the cluster, and the detections were derived within a diameter reported in Table 3. The triangles are the clusters reported in HBvM, corrected to 0.3–3.5 keV X-ray luminosities.

exclude the possibility that most, if not all, of these clusters may be CF clusters at some low level of  $\dot{M}$ .

In Figure 5,  $L_{H\alpha}$  is plotted against the corrected  $L_x$  for the EMSS clusters, together with the luminosities of low- $z$  clusters from HBvM for comparison, corrected to  $H_0 = 50$  km s<sup>-1</sup> Mpc<sup>-1</sup>. One can see that  $L_x$  is only very roughly correlated with  $L_{H\alpha}$ , as previously found, and that the HBvM and EMSS samples occupy the same area of this plot.

Employing the statistical method described in Chamaroux (1987) that utilizes information contained in upper limits as well as detections, we calculate a “true” distribution of  $L_{H\alpha}/L_x$  for our sample. The luminosity ratios rather than the luminosities are tested in order to eliminate the tendency to find higher luminosities at higher redshifts because of survey flux limitations. We find that this distribution does not change with redshift within the sample, and that  $L_{H\alpha}$  is only weakly correlated with  $L_x$ .

There is no indication that H $\alpha$  is detected more readily in clusters with high X-ray luminosities. The correlation between H $\alpha$  and X-ray luminosities is weak, as we stated above, and the X-ray luminosities of the detections are not statistically higher than those of the nondetections. The average X-ray luminosity of the H $\alpha$  detections from flux in the detection cell is  $(2.4 \pm 2.5) \times 10^{44}$  ergs s<sup>-1</sup>, while the detection-cell average luminosity of the nondetections is  $(1.3 \pm 1.1) \times 10^{44}$  ergs s<sup>-1</sup>. The quoted errors here are the sample standard deviation in the luminosities, not the statistical uncertainties in the individual X-ray luminosities (which are approximately 10% of the total X-ray luminosities).

Using the Kolmogorov-Smirnov (KS) test to compare the distributions of  $L_x$  of the EMSS sample and the HBvM sample, we determined that there is a 25% probability that the HBvM samples of clusters and the sample of EMSS clusters are drawn from the same parent population of X-ray-emitting clusters. (This test is not particularly sensitive to how we correct for flux outside the detection cell.) In contrast, a KS test comparing the X-ray luminosity distributions of X-ray-selected active galactic

nuclei (AGNs) (Maccacaro et al. 1991) and the clusters we observed results in only a 0.2% probability that the X-ray-selected AGN and cluster populations were drawn from the same parent population. The log rank test and the generalized Wilcoxon test (Schmitt 1985) also cannot rule out at a statistically significant level the hypothesis that the  $H\alpha$  luminosities and upper limits and the ratio  $L_{H\alpha}/L_x$  of the EMSS sample and the HBvM sample were drawn from the same parent population. In other words, the clusters in the high-redshift sample have similar properties ( $L_x$ ,  $L_{H\alpha}/L_x$ ) to those of the clusters in a low-redshift sample.

#### 6. TOWARD A COMPLETE FLUX-LIMITED SAMPLE

X-ray selection is by far the best way to find distant clusters of galaxies. Optical selection techniques are hampered by contamination of foreground and background galaxies, and by the difficulties inherent in defining the spatial correlation of objects quantitatively. Extended X-ray emission unambiguously identifies a cluster of galaxies. However, X-ray selection of clusters is not free of biasing.

It is important in any examination of a complete sample of objects to consider carefully the selection effects inherent in the sample. Furthermore, in this particular case of the *Einstein* sample, it is important to explore these issues extremely carefully because subsequent X-ray imaging surveys (*ROSAT*) with a similar spatial resolution will have similar limitations. The EMSS survey has also recently been used to construct luminosity functions at different epochs (Paper I), and so a thorough examination of the completeness of this sample is warranted.

As we mentioned in § 2, the EMSS is not, strictly speaking, a flux-limited sample of clusters, but rather is limited by peak surface brightness. And since clusters vary widely in their surface brightness distributions (JF1984), the EMSS cluster sample is not flux-limited over its entire redshift range. A bias in the type of cluster detected can thus occur as long as the X-ray emission is resolved by the detector and the detection algorithm (i.e., detection cell size and background-fitting algorithm) is optimized for the detection of point sources. Clusters with very sharp peaks in their X-ray surface brightness are more readily detected (e.g., CF clusters), while low surface brightness sources with large angular extent will be missed. This latter type of cluster (e.g., Pegasus I; Canizares et al. 1986) is thought to be relatively unevolved and dynamically young (JF1984), with the majority of the X-ray emission arising from the hot coronae of individual galaxies. Pegasus I is an example of a cluster whose X-ray emission was missed by the standard detection algorithm and was found to be present only after a detailed, nonstandard analysis. Another type of cluster that will be missed at intermediate redshifts is Coma-like clusters. These are clusters that are intrinsically bright and regular, but their surface brightness profiles are shallow, with core radii exceeding 500 kpc. Thus, for studies requiring a flux-limited sample, we must take into account the spatial variations of the surface brightness of X-ray-emitting clusters in order to correct our surface brightness-limited sample to a flux-limited sample.

This sort of correction analysis has already been attempted by Pesce et al. (1990) in a general fashion and by Paper I specifically for the EMSS. But no current analysis (not Pesce et al. 1990, Paper I, or the present paper) can be completely conclusive because the detailed distribution of X-ray cluster morphologies in the EMSS sample is not yet known—to say

nothing of the morphologies of clusters missed, if any, by the EMSS (i.e., present within the survey area and with a total X-ray flux greater than the limit but not detected). What each analysis attempts to do is to estimate the spatial distribution of X-ray flux for distant clusters based upon the observed structure of nearby ones, and then correct the fluxes and numbers for the missing amounts. Three questions must be addressed concerning the EMSS: How are flux estimates affected if the entire cluster X-ray emission is not contained within the detection cell? How do we estimate the morphological characteristics of this sample? And, most important, how many and what type of clusters are missed with this selection technique?

In § 6.1 we show that some non-CF clusters have small X-ray core radii, so that the EMSS is not necessarily dominated by CF clusters as suggested by Pesce et al., and we suggest that many clusters with large core radii may have low luminosity, and thus would be excluded by the flux limit. In § 6.2 we show that the relative flux corrections between the low- and high-redshift bins are minimal, and thus our new assumption about X-ray morphologies within the EMSS does not alter the result of a decreasing cluster X-ray luminosity function with redshift presented in Paper I. In § 6.3 we demonstrate that even though we use a different derived mean surface brightness distribution for EMSS clusters (nearly a factor of 2 smaller scale size than assumed in Paper I), the low-redshift luminosity function of Paper I is in agreement with the luminosity functions of Piccinotti et al. (1982) and Edge et al. (1990), which were constructed using data from nonimaging X-ray telescopes. This agreement implies that the EMSS misses very few clusters as a result of their distended X-ray emission. We then place an upper limit on the fraction of clusters excluded from the EMSS because of morphology, and examine the consequences of this level of exclusion for our results.

#### 6.1. Core Sizes for Cooling Flows and Non-Cooling Flows

We can improve our flux estimate from a uniform correction over the entire sample (as in Paper I) by using two different corrections, one for CF and another for non-CF clusters, and so also estimate how preferentially CF clusters are detected over non-CF clusters by the IPC. Even in our sample, the non-CF clusters seem somewhat larger than the clusters with CFs (Henry et al. 1991). In order to compare the sizes of CF and non-CF clusters, we analyzed a comparison sample of clusters which were studied by both JF1984 and Arnaud (1988). JF1984 contains morphological data for a sample of 46 clusters observed with the IPC. Arnaud (1988) determined whether or not 104 clusters observed by the IPC were CFs. We used the Arnaud analysis to divide the JF1984 sample into CF and non-CF clusters.

We compared the distribution of  $\alpha_{\text{Mpc}}$  in the CF and the non-CF clusters with a KS test and found that the probability that the two distributions have the same parent distributions is 12%. Although this does not rule out the possibility that the two distributions have identical parent distributions, we will continue to treat these two types of clusters independently in this paper. Upon inspection of the two distributions (see Fig. 6), the means of the two samples differ only because the non-CF cluster distribution has a high  $\alpha_{\text{Mpc}}$  tail. The median values for these two samples are 0.20 and 0.25 Mpc, respectively.

JF1984 found excesses above their  $\beta$ -models for CFs which have a median value of approximately 10% of the total  $L_x$  (values range from 0% to 30%). Thus we have corrected the

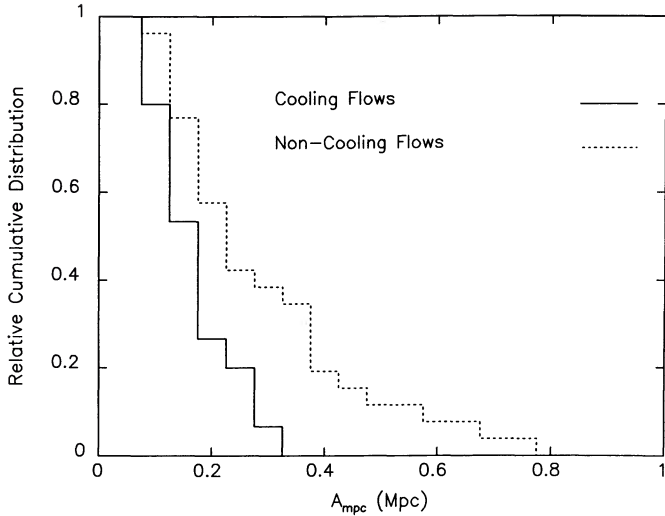


FIG. 6.—Relative cumulative distribution of CF (solid lines) and non-CF (dashed lines) core radii ( $a_{\text{Mpc}}$ ) for the subsample of 41 clusters analyzed both by JF1984 and by Arnaud (1988). Note that the median  $a_{\text{Mpc}} = 0.2$  Mpc, and that only 10%–20% of non-cooling flow clusters have core radii larger than 0.4 Mpc. The probability that the CF and non-CF clusters were drawn from the same parent population is 12%.

X-ray luminosities of the EMSS clusters to account for flux outside the detection cell by assuming  $a_{\text{Mpc}} = 0.20$  Mpc plus a central excess of 10% for all CF clusters and  $a_{\text{Mpc}} = 0.25$  Mpc for all non-CF clusters. The corrected X-ray luminosities using these  $\beta$ -models are listed under  $L_x(\text{Corrected})$  in Table 2.

Although we did not necessarily identify all of the CFs in our sample, the error in our flux calculation for CF and non-CF clusters is not large. Figure 6 shows that CF and non-CF clusters have similar size distributions, so even if we have incorrectly classified a few EMSS clusters as CF or non-CF, the resulting errors in flux correction are modest (inasmuch as separating the sample into only two groups leads to flux errors for those individual clusters which differ significantly from the mean).

Also, the bias toward detecting CF over non-CF clusters is not large, because many non-CF clusters have small core radii and the non-CF clusters with large core radii tend to be low luminosity. Specifically, the CF and non-CF cluster distributions in Figure 6 differ only in that 20% (five clusters) in the non-CF cluster distribution have large  $a_{\text{Mpc}}$  values ( $> 0.4$  Mpc). Three of these five have  $L_x \leq 5 \times 10^{43}$  ergs  $\text{s}^{-1}$ , well below the X-ray luminosities of all but one (MSS 1531.2+3118, not in the flux-limited sample) of the EMSS clusters in our sample. Further, the previous example of a very low surface brightness cluster (Pegasus I) whose X-ray emission was missed by the standard detection algorithm has  $L_x \approx 10^{42}$  ergs  $\text{s}^{-1}$ . This low luminosity would not have been detected beyond  $z \sim 0.03$  even if all of the X-ray emission from Pegasus I were concentrated into a single point source. Therefore, from the statistics in JF1984 and Arnaud (1988), it is clear that many non-CF clusters have small radii, so that the bias in favor of CFs in imaging X-ray telescope surveys is not large. Also, the large  $a_{\text{Mpc}}$  non-CF sample may be dominated by low  $L_x$  objects which would not be detected in X-ray imaging surveys even if they were more compact.

Unfortunately, our analyses are not completely compelling, because, for example, the JF1984 sample is not a complete, flux-limited sample (to say nothing of the Arnaud 1988 studied

subsample of JF1984). These clusters were selected because they could be well studied with the IPC, so more diffuse clusters may have been specifically excluded. For example, the well-studied Coma Cluster has  $L_x = 5.13 \times 10^{44}$ ,  $z = 0.0232$ , and  $a_{\text{Mpc}} \sim 0.50$  (Abramopoulos & Ku 1983). Coma would not have been detected by the REV 1 detection algorithm at  $z \gtrsim 0.1$  for a detection cell flux limit of  $8 \times 10^{-13}$ . Since we do not know how common Coma-like clusters are at intermediate redshifts ( $z \sim 0.1$ – $0.2$ ), we cannot know how to correct our sample for the number of clusters missed. We specifically readdress the completeness of our sample in § 6.3 below.

An independent analysis of cluster sizes by Henry et al. (1991) supports the smaller  $a_{\text{Mpc}}$  values found in our work. Using IPC data both for extended sources found within the EMSS and for a large sample of clusters detected with non-imaging X-ray telescopes compiled by Edge et al. (1990), Henry et al. (1991) also finds  $a_{\text{Mpc}} \approx 0.25$  Mpc. A study by Henriksen (1992) of a complete sample of 25 nearby Abell clusters with  $D \leq 2$  finds average core radii of  $0.25 \pm 0.14$  Mpc, and finds that 30% have CFs. He also finds that five out of the six clusters with core radii of 0.4 Mpc have low X-ray luminosities ( $L_x \leq 6 \times 10^{43}$  ergs  $\text{s}^{-1}$ ), which suggests that Coma-like clusters may not be very common.

## 6.2. Estimating EMSS Cluster Morphology and X-Ray Flux Corrections

Paper I analyzes the EMSS sample of clusters to determine the X-ray luminosity function in bins of redshift and concludes that the most X-ray luminous clusters have declined in numbers in the recent past ( $z < 0.6$ ). While the result in Paper I required a correction of the sort we are discussing here, the redshift range ( $z < 0.14$ ) where this correction is the greatest (i.e., most clusters are resolved by the IPC regardless of structure) was not used in the analysis. Also, when comparing adjacent redshift bins, the differential correction, not the absolute correction, is important. The actual corrections to the point-source fluxes of EMSS clusters based upon  $\beta$ -models with the different core radii are shown in Figure 7. This figure

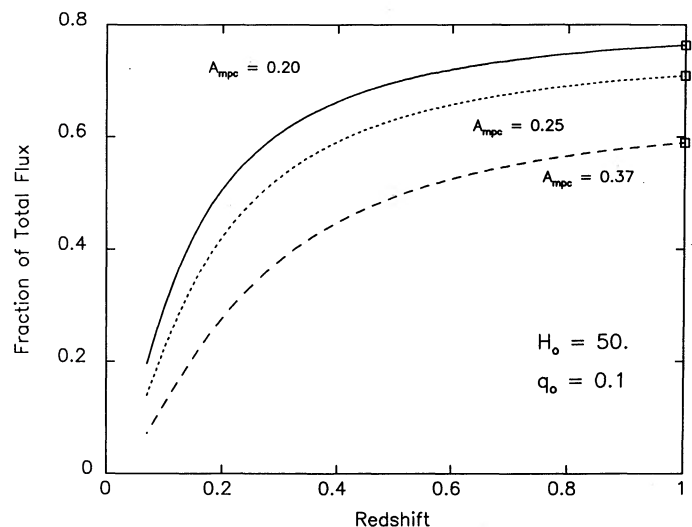


FIG. 7.—Fraction of total cluster X-ray flux in a  $2.4 \times 2.4$  detection cell as a function of redshift. We assume  $q_0 = 0.1$  and  $H_0 = 50 \text{ km s}^{-1} \text{ Mpc}^{-1}$ . This is a graphical representation of equation (1) of Paper I for three values of  $a_{\text{Mpc}}$  as discussed in the text. Note that the correction is not a strong function of redshift for  $z > 0.2$ .

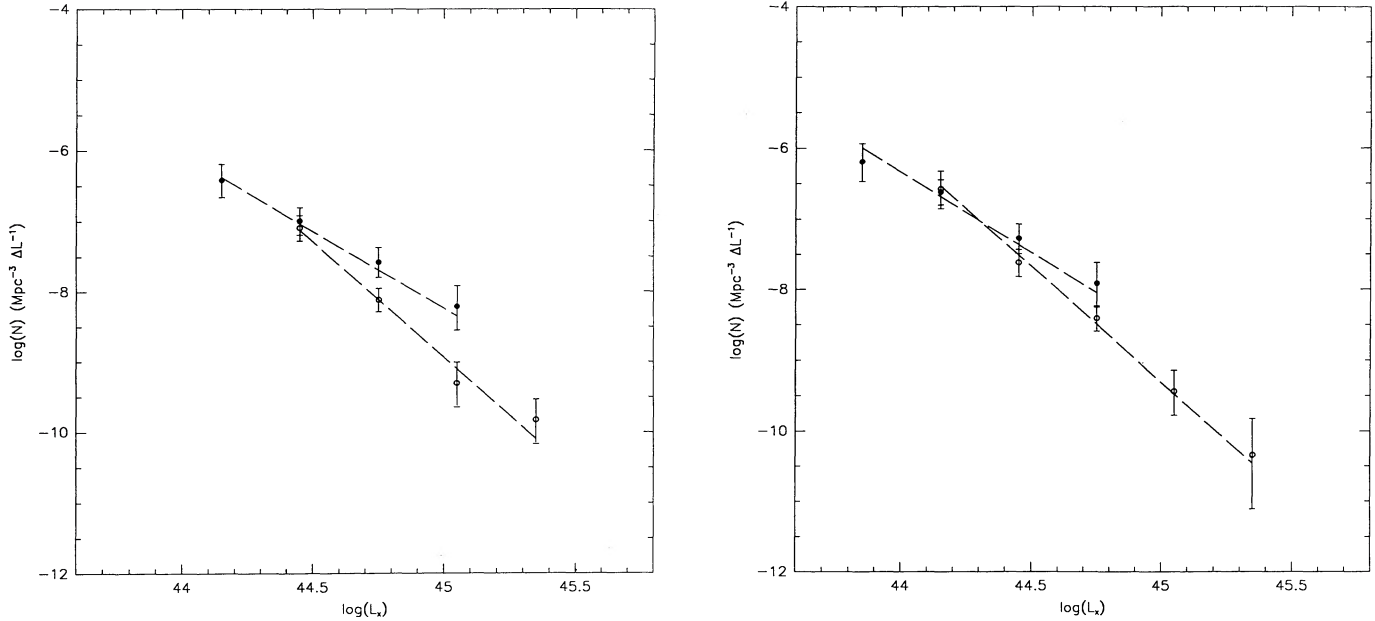


FIG. 8.—*Left*: X-ray luminosity function for the low-redshift shell (*filled circles*) and the high-redshift shell (*open circles*) derived for the EMSS in Paper I (assuming core radii of 370 kpc and  $q_0 = 0$ ). *Right*: The same comparison, but derived for assumed core radii of 200 kpc suggested from our analysis herein. Changing the assumptions on cluster core size does not change the general result of Paper I that there are fewer high X-ray luminosity clusters at high redshift.

explicitly shows that for all  $a_{\text{Mpc}}$  values, the absolute flux corrections are somewhat large for  $z > 0.14$  but the relative corrections between redshift bins for  $z = 0.14$  to  $z = 0.6$  are modest, i.e., a factor of 2 or less. Finally, the size of the correction made in Paper I is larger than the amount we suggest to use herein, because we find smaller cluster sizes ( $\langle a_{\text{Mpc}} \rangle = 0.37$  values in Fig. 7 compared with those for  $\langle a_{\text{Mpc}} \rangle = 0.20$ – $0.25$ ).

By assuming that all of the EMSS X-ray fluxes should be corrected for sizes of  $\sim 0.20$  Mpc rather than  $\sim 0.37$  Mpc, the main result of Paper I remains unchanged, as shown in Figure 8. On the left are the high- and low-redshift luminosity functions from Paper I assuming flux corrections based upon 0.37 Mpc; on the right are the same data assuming 0.20 Mpc sizes for the sample. The assumption of 0.20 Mpc core size for the entire sample is, in our opinion, an extreme assumption. This assumption would imply that all EMSS clusters are as compact as typical CF clusters seen nearby. Even with these two extreme assumptions ( $a_{\text{Mpc}} = 0.37, 0.20$ ), the result of fewer high- $L_x$  clusters at high  $z$  remains present at the  $3\sigma$  significance level per point. Henry et al. (1991) have independently come to the same conclusion.

### 6.3. Completeness of the EMSS Sample

To address the question of whether the EMSS systematically misses many clusters, we can compare the luminosity function (LF) computed from a nearby X-ray flux-limited (*HEAO 1*, thus nonimaging) sample (Edge et al. 1990) and the Piccinotti et al. (1982) LF with the LF computed for the redshift range 0.14–0.20 in the EMSS sample (Gioia et al. 1990a). We find that the two luminosity functions are identical to within the errors (see Fig. 9), if we correct the EMSS fluxes for flux extended outside the detection cell using  $a_{\text{Mpc}} = 0.20$  (*triangles*) rather than 0.37 (*crosses*). This result suggests that the EMSS misses far fewer clusters than has previously been supposed (Pesce et al. 1990). If the EMSS is missing many clusters at redshifts of 0.14 and greater, then the nonimaging *HEAO 1*

sample must also be missing many low-redshift X-ray clusters ( $z < 0.1$ ). The agreement in luminosity functions shown in Figure 9 validates the cluster size analysis using the heterogeneous JF1984 samples made in § 6.1 above.

The Paper I flux correction using  $a_{\text{Mpc}} = 0.37$  agrees with the Piccinotti et al. result only at the  $3\sigma$  level (error bars are  $2\sigma$  high at each luminosity bin) and thus can be excluded at a high

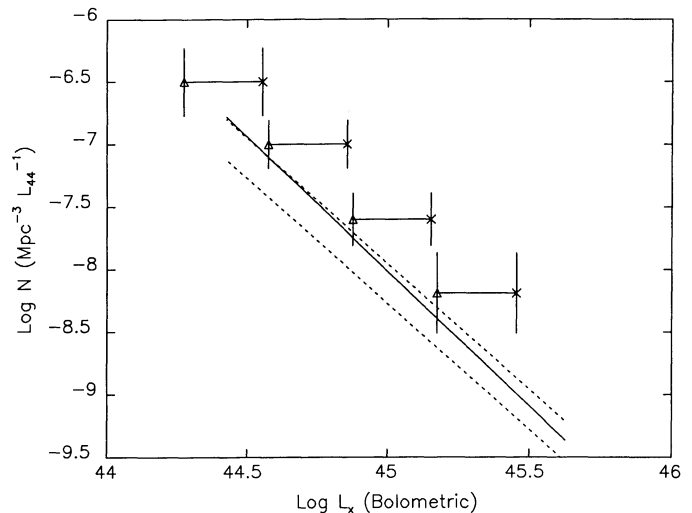


FIG. 9.—X-ray luminosity function for EMSS clusters with redshifts between 0.14 and 0.20. Crosses represent the luminosities if  $a_{\text{Mpc}} = 0.37$  for all clusters. Triangles are the luminosities if  $a_{\text{Mpc}} = 0.20$  and  $L_x(\text{excess}) = 0.10$  of the total X-ray luminosity for all clusters (i.e., as if all clusters are CF clusters). In order for the EMSS result to be in agreement with the LF result of Edge et al. (1990) (the range is represented by dashed lines) and Piccinotti et al. (1982) (*solid line*), the fluxes of the EMSS must be corrected by an amount consistent with a parent population of compact, centrally condensed clusters ( $a_{\text{Mpc}} = 0.20$ – $0.25$ ). The fluxes of each luminosity function were corrected to bolometric by assuming  $T_x = 6$  keV.

confidence level ( $>99\%$ ) unless there is strong “positive” number/luminosity evolution for clusters between  $z = 0$  and  $z = 0.2$ , despite the “negative” evolution at higher redshifts (but this has not been seen in other samples; e.g., Henry & Lavery 1984). The Edge et al. (1990) sample is somewhat heterogeneous and is used here because it is in agreement with the Piccinotti *et al.* (1982) results.

In conclusion, we find that the X-ray LF derived from the EMSS’s lowest redshift shell is consistent with the lower redshift X-ray LFs derived in earlier studies (Piccinotti et al. 1982; Edge et al. 1990) if we correct the EMSS fluxes for flux lost from outside the detection cell for an assumed size of 0.20 Mpc. This agreement seems to indicate that the EMSS does not miss many clusters entirely. The distribution of cluster sizes in JF1984 suggests that the EMSS may miss  $\sim 10\%$  of the cluster population, and that these missed clusters are the spatially very distended, unevolved clusters without CF ( $\sim 7\%$  of the JF1984 sample have  $a_{\text{Mpc}} \geq 0.5$  Mpc). Therefore, we agree qualitatively, but not quantitatively, with the result of Pesce et al. (1990).

We can further conclude that since the EMSS luminosity function at low redshifts seems to be substantially the same as other low-redshift luminosity functions (Piccinotti et al. 1982; Edge et al. 1990), then the underlying population of clusters must have a high fraction that are centrally condensed but are not necessarily CF clusters. The EMSS does not miss clusters with  $a_{\text{Mpc}} \geq 0.5$  Mpc, which may be 10% of the total population of non-CF clusters at low redshifts. Thus a *slight* bias toward the detection of clusters with cooling flows exists in the EMSS, since CF clusters do not tend to have  $a_{\text{Mpc}} \geq 0.5$ . One may correct the fraction of detected clusters which are CFs to the true fraction of CFs by the following formula:

$$f = \frac{f_{\text{CF}}(1 - f_{\text{miss}})}{1 - f_{\text{CF}} f_{\text{miss}}}, \quad (2)$$

where  $f_{\text{CF}}$  is the fraction of detected clusters with CFs,  $f$  is the fraction of all clusters with CFs, and  $f_{\text{miss}}$  is the fraction of non-CF clusters which will be missed by the imaging surveys.

Table 4 lists the fraction of CFs detected in our sample as a function of  $z$ , and the corrected fraction due to the estimated 10% of all clusters which may have been missed altogether. The numbers in Table 4 include those clusters detected in the EMSS below the point-source flux limit but whose extended fluxes would have included them in the sample (this slightly decreases the CF percentage in each redshift bin).

TABLE 4  
COOLING FLOW FRACTION WITH REDSHIFT

Redshift Range	Number Detected in H $\alpha$ /Total	Corrected Percentage <sup>a</sup>
0.065–0.14 .....	4/13	$\geq 30\%$
0.14–0.20 .....	2/6	$\geq 33\%$
0.20–0.37 .....	5/9	$\geq 56\%$
0.01–0.46 .....	46/107 <sup>b</sup>	30% <sup>c</sup>

<sup>a</sup> Detection percentage corrected assuming that 10% of all clusters are missed by the REV 1 detection algorithm and that all of the missed clusters are non-CF clusters.

<sup>b</sup> Arnaud 1988: A sample of mostly low-redshift (only 14 have  $z \geq 0.2$ ) X-ray clusters observed with the IPC with cooling times less than  $2 \times 10^{10}$  yr.

<sup>c</sup> Percentage corrected for the assumption that only 70% of CFs have H $\alpha$  emission.

The fraction of CFs found by Arnaud (1988) in a predominantly low-redshift sample is not directly comparable to the numbers from our survey because not all of the CFs found by the X-ray deconvolution method would be detected in a H $\alpha$  imaging survey. In Table 4, the last item, we correct the fraction of CFs at low redshift found by X-ray deconvolution methods to the fraction that would be detected in a deep H $\alpha$  survey by the H $\alpha$  detection percentage of the HBvM sample described in § 5. The resulting value of 30% is comparable to the percentage of CFs found in the lowest redshift bin in our survey. Because the higher redshifts for our clusters require a larger H $\alpha$  minimum detectable luminosity, we should miss more CFs than did the compilation by HBvM, based upon HBvM’s detected H $\alpha$  luminosities. So at  $z \sim 0.2$  we should have seen only the brightest 32% of the CFs in our sample. Therefore, we have listed the converted H $\alpha$  detection percentages as *lower limits* to the true CF percentage in the EMSS sample.

Thus we conclude that we cannot rule out that most, if not all, of the highest redshift clusters in our sample are CFs at clusters at some level, because our H $\alpha$  observations are not sensitive enough to detect as many CFs as for nearby clusters (e.g., HBvM) and because, even for very nearby clusters, not all CFs have detectable H $\alpha$  emission. *But this conclusion is not necessarily the result of a selection effect due to the detection method as suggested by Pesce et al. (1990)*, since up to 80% of non-CF clusters also have core radii smaller than 0.4 Mpc, making most non-CF clusters as easy to detect as CFs, and since clusters with large core radii are systematically less luminous than clusters with small core radii. Therefore, even if we account for the exclusion of 10% of all clusters due to large core radii (and thus do not have cooling flows), the fraction of clusters with extended H $\alpha$  emission among X-ray-emitting clusters was considerably higher at  $z \geq 0.2$  than in the present. Based upon the very modest statistics in our survey and assuming that the fraction of CFs with H $\alpha$  emission remains constant in time, the percentage of CFs among X-ray-emitting clusters was at least twice as great at  $z > 0.2$  as at  $z < 0.1$ .

## 7. EVOLUTION

As can be seen from the small numbers in Table 4, the results of any test for the cosmological evolution of CFs based upon the current small sample will not have high statistical significance. However, because the EMSS offers the only complete sample of high- $z$  X-ray-selected clusters which will be available for several years, the results of a standard  $\langle V_e/V_a \rangle$  test for evolution in a flux-limited sample (Schmidt 1968; Avni & Bahcall 1980) are in order (see Table 5). As we show below, we have selected our CF and non-CF samples in such a way as to *minimize* the difference between the values in Table 5, ensuring that systematic error only separates the two values of  $\langle V_e/V_a \rangle$ . However, owing to the small numbers in our sample which preclude a statistically significant difference in Table 5, we can only suggest that CF and non-CF clusters may exhibit differing cosmological evolution.

TABLE 5  
 $\langle V_e/V_a \rangle$  TEST FOR EMSS COOLING FLOWS  
AND NON-COOLING FLOWS

Cooling Flows	Non-Cooling Flows
$0.52 \pm 0.10$	$0.39 \pm 0.07$

For each cluster in the CF and non-CF cluster samples, the enclosed and accessible volumes were computed in the standard manner by taking into account the varying sky coverage as a function of X-ray flux for the EMSS (Gioia et al. 1990b). Luminosities for each cluster were computed by assuming  $H_0 = 50 \text{ km s}^{-1} \text{ Mpc}^{-1}$  and  $q_0 = 0.1$ ; a standard  $\beta$ -model for the X-ray flux distribution with  $\beta = 0.67$  and  $a_{\text{Mpc}} = 0.20$  and 10% central excess for the CF and  $a_{\text{Mpc}} = 0.25$  for the non-cooling flows. Parameter choices were discussed in § 6.1.  $K$ -corrections were made for band width and spectral slope assuming a power-law spectral index of  $-0.5$ . A correction for Galactic hydrogen absorption has already been applied to the fluxes (Gioia et al. 1990b). The maximum distance at which the cluster could have been detected is computed using the total computed luminosity of the cluster distributed spatially by a  $\beta$ -model in order to determine the amount of flux visible in a single IPC detection cell.

The most difficult decision for this test for evolution is how to choose the sample on which to perform the test. To be included in the CF sample, the CFs identified herein require not only an X-ray flux above our limit but also an  $H\alpha$  detection which has no single flux limit, and so certainly no single luminosity limit, given the very different redshifts present. To simply compute a maximum volume in which the CFs could be detected based upon the observed  $H\alpha$  luminosities is not correct, because the entire sky area of the EMSS was not surveyed in  $H\alpha$  to produce an independent limiting volume in the manner described by Avni & Bahcall (1980). However, if this were done, only three CF clusters (MS 1050.7+4946, MS 1754.9+6803, and MS 2348.0+2913) would be limited by their  $H\alpha$  detections rather than their X-ray detections. We have removed these three clusters from the CF sample and use only those CFs whose  $H\alpha$  luminosities are so large that they would have been detected even at the maximum detection distance determined from their X-ray fluxes. If these three were included in the CF sample, and their maximum volumes computed using the  $H\alpha$  measurements as prescribed by Avni & Bahcall (1980), the values of  $\langle V_e/V_a \rangle$  in Table 5 would be substantially higher (0.63). Therefore, the values in Table 5 use only the X-ray fluxes and redshifts for the clusters and the X-ray flux limits of the EMSS.

By the method we have chosen, only the most luminous CFs are retained in the CF sample; weak or undetectable (by the  $H\alpha$  method) CFs may also be present in the non-CF sample, especially at high redshifts as we have mentioned previously. The limiting  $H\alpha$  luminosity for undetected clusters increases quickly with redshift owing to their distance, decreased CCD quantum efficiency, decreased filter throughputs at longer wavelengths, and increased sky noise due to night-sky emission lines. All clusters may be CF clusters at some level; what we have done here is to select CFs on the basis of detectable  $H\alpha$  emission. If  $H\alpha$  emission is an unbiased indicator of a CF, i.e., the percentage of CFs with luminous  $H\alpha$  emission remains constant with redshift (e.g., if  $\sim 70\%$  of all CFs are luminous  $H\alpha$  emitters regardless of redshift), then we have defined our CF sample in a reasonable way.

So the CF  $\langle V_e/V_a \rangle$  value in Table 5 must be treated as a lower limit because high-redshift CFs are still preferentially missed by the  $H\alpha$  survey compared with nearby ones. Because of the correlation between X-ray flux and redshift for this sample, including these objects as non-CF rather than CF decreases  $\langle V_e/V_a \rangle$  for the CFs and increases this statistic for the non-CF clusters. In other words, our failure to detect these

high- $z$  CFs in  $H\alpha$  only serves to move the two values in Table 5 closer together. Therefore, the difference in the type of cosmological evolution of CF and non-CF clusters can only be larger than as shown in Table 5. The systematic errors, if minimized, could only move the values for  $\langle V_e/V_a \rangle$  for the CF and non-CF samples farther apart.

Based upon the results of Paper I (verified in § 6.2 above for a range of cluster sizes), the cluster sample as a whole exhibits “negative” cosmological evolution. Here and in the previous section, we have shown in two ways that CF clusters are either constant in number/luminosity with redshift, or may even have “positive” cosmological evolution (when the CF and non-CF values in Table 5 are treated as lower and upper limits, respectively). Thus the non-CF (or non-CF plus weak-CF) clusters may be decreasing in numbers/luminosity with redshift (into the past) even faster than found in Paper I.

This result agrees qualitatively with the suggestion by Edge et al. (1990) that the evolution in clusters may be brought about by cluster collisions, so that low-luminosity clusters merge to form high-luminosity clusters. This merging may also disrupt the cooling flow process, so that CF clusters appear to decrease in number/luminosity with cosmological time. Alternatively, mergers may enhance the inhomogeneity of the flow, thus reducing the production of optical emission lines in CFs (Voit & Donahue 1990).

## 8. CONCLUSION

The detection of  $H\alpha$  emission in many X-ray-emitting clusters at relatively high redshifts is strong for a large population of cooling flow clusters in the past. Since we show that cooling flows exist at high redshift, we may surmise that cluster cooling flows are persistent phenomena. If cooling flows were a recent or a sporadic event (Meiksin 1990), we would not expect to see very many of them at high redshift. Because we do see them, we compound the mystery of the following question: if these flows persist at a high level of  $\dot{M}$ , where does the cooled mass hide? Partial answers may be either that not all of the  $\dot{M}$  reaches the central CF cluster galaxy (see Fabian et al. 1984, 1991) or that low-mass star formation predominates in these galaxies (see Sarazin 1988). Either supposition is supported by the recent observational work of McNamara & O’Connell (1989) and Romanishin (1986), who suggest that a young stellar population may exist in these galaxies, but at a level which only explains the destination of approximately 10% of the mass in the cooling flow. The fate of 90% of the cooling mass remains to be revealed.

The emission-line luminosities are correlated with the X-ray luminosities of the clusters in the distant sample in the same manner as the emission-line and X-ray luminosities of the nearby clusters in HBvM. Statistical tests comparing the two samples suggest that the two samples were drawn from similar parent populations. These results suggest that the intrinsic properties of cooling flows at substantial redshifts ( $z \sim 0.2\text{--}0.3$ ) are similar to the cooling flows nearby. Further study, such as long-slit optical spectroscopy and deeper  $H\alpha$  images (sufficient to detect  $L_{H\alpha} \lesssim 10^{41} \text{ ergs s}^{-1}$ ), is required to confirm this similarity in detail.

We find that when we account for the expected differences in the spatial extent of the X-ray emission of CF and non-CF clusters, the conclusion of Paper I that X-ray-luminous clusters have decreased in number and/or luminosity since  $z \sim 0.3$  is not changed. In addition, we find that the fraction of X-ray clusters with optical filaments, and, by inference, those with

CFs, appears to be at least a factor of 2 higher at  $z \gtrsim 0.2$  than at lower redshifts. When we compare the results of a  $\langle V_e/V_a \rangle$  test for the clusters in which we detected H $\alpha$  with the results for the clusters in which we did not, we find that the evolutionary characteristics of the two samples differ by at least  $1 \sigma$ . Our conservative sample choice and the limitations on detection of CFs at high redshift have brought the two estimates for  $\langle V_e/V_a \rangle$  closer together. Thus we make only the tentative suggestion that the number and/or luminosity of clusters with CFs stays constant, or increases with lookback time, in contrast to the number and/or luminosity of non-CF clusters, which decreases with lookback time.

Additionally, the selection effects inherent in a survey of extended objects such as the EMSS cluster survey are not trivial but have been taken into account in this analysis. The most important assumption is that of the "average" underlying surface brightness distribution of the sample. We have found that in order for the low-redshift X-ray luminosity function derived from the EMSS sample to agree with other low-redshift X-ray luminosity functions constructed from samples obtained with nonimaging telescopes, we needed to assume that CF clusters have core radii of  $\sim 0.2$  Mpc and non-CF clusters have average core radii of  $\sim 0.25$  Mpc. We were not, however, forced to assume that most EMSS clusters are cooling flow clusters as in Pesce et al., because many non-CF clusters, also have small core radii (JF1984; Arnaud 1988).

The agreement of the low-redshift LFs derived from the non-imaging survey (Piccinotti et al. 1982; Edge et al. 1990) and the EMSS indicates that the EMSS does not miss many clusters. (We note here that changing the assumption of core size *reduced* the original EMSS LF of Paper 1, so that the original LF contained a *higher* density of clusters at a given luminosity,

in disagreement with Piccinotti et al. 1982.) We estimated that only  $\sim 10\%$  of all clusters have core radii of 0.5 Mpc or more, rendering them difficult to detect or invisible to the EMSS survey. Thus, the EMSS is rich in distant CFs, not because of a selection effect but because CF clusters were a larger percentage of X-ray-emitting clusters in the past than they are today.

Future studies with better spatial resolution and sensitivity can establish the distribution of surface brightness morphologies in distant clusters in order to better estimate the total X-ray fluxes and completeness of X-ray-selected samples of clusters of galaxies like the EMSS sample of clusters. The lower detection background present in the *ROSAT* position-sensitive proportional counter (PSPC) will allow a more detailed study of cluster detectability as a function of detection cell size than was possible with the *Einstein* IPC. Such studies can confirm the results presented herein.

We thank the EMSS team (specifically Tommaso Maccaro, Simon Morris, Rudy Schild, and Anna Wolter) for use of their data prior to publication. We would like to acknowledge the data and analysis tables for IPC X-ray clusters supplied by Keith Arnaud and helpful discussions with Andy Fabian and Mike Shull. We wish to thank the NOAO staff for assistance in data reduction, in particular Jeannette Barnes and Brett Goodrich. M. D. acknowledges support from NASA Graduate Student Research Fellowships and the Boettcher and Zonta Foundations. J. S. would like to acknowledge support from grants NAG5-1224, AST8715983, and AST8820416. I. M. G. acknowledges partial support from NASA contract NAS8-30751 and from Smithsonian Institution scholarly studies grant SS88-3-87.

## REFERENCES

- Abramopoulos, F., & Ku, W. H.-M. 1983, *ApJ*, 271, 446  
 Arnaud, K. A. 1988, in *Cooling Flows in Galaxies and Clusters*, ed. A. Fabian (Cambridge: Cambridge Univ. Press), 31  
 Avni, Y., & Bahcall, J. N. 1980, *ApJ*, 235, 694  
 Baum, S. A. 1987, Ph.D. thesis, Univ. Maryland  
 Baum, S. A., Heckman, T. M., Bridle, A. H., van Breugel, W. J. M., & Miley, G. L. 1988, *ApJS*, 68, 833  
 Begelman, M., & Fabian, A. C. 1990, *MNRAS*, 244, 26P  
 Binney, J., & Cowie, L. L. 1981, *ApJ*, 247, 464  
 Bothun, G. D. 1986, in *Santa Cruz Summer Workshop, Nearly Normal Galaxies*, ed. S. M. Faber (New York: Springer-Verlag), 184  
 Bothun, G. D., Impey, C. D., Malin, D. F., & Mould, J. R. 1987, *AJ*, 94, 23  
 Butcher, H., & Oemler, A. Jr. 1984, *ApJ*, 285, 426  
 Canizares, C. R., Clark, G. W., Jernigan, J. G., & Markert, T. H. 1982, *ApJ*, 262, 33  
 Canizares, C. R., Clark, G. W., Markert, T. H., Berg, C., Smedira, M., Bardas, D., Schnopper, H., & Kalata, K. 1979, *ApJ*, 234, L33  
 Canizares, C. R., Donahue, M., Fabbiano, G., Stewart, G. C., & McGlynn, T. A. 1986, *ApJ*, 304, 312  
 Canizares, C. R., Markert, T. H., & Donahue, M. 1988, in *Cooling Flows in Galaxies and Clusters*, ed. A. Fabian (Cambridge: Cambridge Univ. Press), 63  
 Canizares, C. R., Stewart, G. C., & Fabian, A. C. 1983, *ApJ*, 272, 449  
 Chamaroux, P. 1987, *A&A*, 177, 326  
 Cowie, L. L., Hu, E. M., Jenkins, E. B., & York, D. G. 1983, *ApJ*, 262, 29  
 Crawford, C. S., & Fabian, A. C. 1989, *MNRAS*, 239, 219  
 David, L. P., Bregman, J. N., & Seab, C. G. 1988, *ApJ*, 329, 66  
 Donahue, M., & Voit, G. M. 1991, *ApJ*, 381, 361  
 Draine, B. T., & Lee, H. M. 1984, *ApJ*, 285, 89  
 Edge, A. C., Stewart, G. C., Fabian, A. C., & Arnaud, K. A. 1990, *MNRAS*, 245, 559  
 Fabian, A. C., Arnaud, K. A., Nulsen, P. E. J., & Mushotzky, R. F. 1986, *ApJ*, 305, 9  
 Fabian, A. C., & Nulsen, P. E. J. 1977, *MNRAS*, 180, 479  
 Fabian, A. C., Nulsen, P. E. J., & Canizares, C. R. 1984, *Nature*, 310, 733  
 ———. 1991, *Astron. Astrophys. Rev.*, 2, 191  
 Gioia, I. M., Henry, J. P., Maccacaro, T., Morris, S. L., Stocke, J. T., & Wolter, A. 1990a, *ApJ*, 356, L35 (Paper I)  
 Gioia, I. M., Maccacaro, T., Schild, R. E., Wolter, A., Stocke, J. T., Morris, S. L., & Henry, J. P. 1990b, *ApJS*, 72, 567  
 Heckman, T. M. 1981, *ApJS*, 250, L59  
 Heckman, T. M., Baum, S., van Breugel, W., & McCarthy, P. 1989, *ApJ*, 338, 48  
 Henriksen, M. J. 1992, in preparation  
 Henry, J. P., Gioia, I. M., Maccacaro, T., Morris, S. L., Stocke, J. T., & Wolter, A. 1991, *ApJ*, submitted  
 Henry, J. P., & Henriksen, M. J. 1986, *ApJ*, 301, 689  
 Henry, J. P., & Lavery, R. J. 1984, *ApJ*, 280, 1  
 Hu, E. M., Cowie, L. L., & Wang, Z. 1985, *ApJS*, 59, 447  
 Impey, C., Bothun, G., & Malin, D. 1988, *ApJ*, 330, 634  
 Johnstone, R. M., Fabian, A. C., & Nulsen, P. E. J. 1987, *MNRAS*, 224, 75  
 Jones, C., & Forman, W. 1984, *ApJ*, 276, 38 (JF1984)  
 Maccacaro, T., Della Ceca, R., Gioia, I., Morris, S., Stocke, J., & Wolter, A. 1991, *ApJ*, 374, 117  
 Mathews, W. G., & Bregman, J. N. 1978, *ApJ*, 224, 308  
 McNamara, B. R., & O'Connell, R. W. 1989, *AJ*, 98, 2018  
 Meiksin, A. 1990, *ApJ*, 352, 466  
 Mushotzky, R. F., Holt, S. S., Smith, B. W., Boldt, E. A., & Serlemitsos, P. J. 1981, *ApJ*, 244, L47  
 Nesci, R., Gioia, I. M., Maccacaro, T., Morris, S., Perola, G. C., Schild, R. E., & Wolter, A. 1989, *ApJ*, 344, 104  
 Pesce, J. E., Fabian, A. C., Edge, A. C., & Johnstone, R. M. 1990, *MNRAS*, 244, 58  
 Piccinotti, G., Mushotzky, R. F., Boldt, E. A., Holt, S. S., Marshall, F. E., Serlemitsos, P. J., & Shafer, R. A. 1982, *ApJ*, 253, 485  
 Romanishin, W. 1986, *ApJ*, 301, 675  
 Romanishin, W., & Hintzen, P. 1988, *ApJ*, 324, L17  
 Sandage, A., Binggeli, B., & Tammann, G. A. 1985, *AJ*, 90, 1759  
 Sarazin, C. L. 1986, *Rev. Mod. Phys.*, 58, 1  
 ———. 1988, *X-Ray Emission from Clusters of Galaxies* (Cambridge: Cambridge Univ. Press)  
 Schmidt, M. 1968, *ApJ*, 151, 393  
 Schmitt, J. H. M. M. 1985, *ApJ*, 293, 178  
 Stark, A. A., Heiles, C., Bally, J., & Linke, R. 1984, Bell Laboratories, privately distributed magnetic tape  
 Stewart, G. C., Canizares, C. R., Fabian, A. C., & Nulsen, P. E. 1984, *ApJ*, 278, 576  
 Stocke, J. T., Maccacaro, T., Donahue, M., & Gioia, I. 1992, in preparation  
 Stocke, J. T., Morris, S., Gioia, I., Maccacaro, T., Schild, R., Wolter, A., Fleming, T. A., & Henry, J. P. 1991, *ApJS*, 76, 813  
 Stone, R. P. S. 1977, *ApJ*, 218, 741  
 Voit, G. M., & Donahue, M. 1990, *ApJ*, 360, L15